VYSOKÉ UČENÍ TECHNICKÉ V BRNĚ
BRNO UNIVERSITY OF TECHNOLOGY

FAKULTA STROJNÍHO INŽENÝRSTVÍ
LETECKÝ ÚSTAV

FACULTY OF MECHANICAL ENGINEERING
INSTITUTE OF AEROSPACE ENGINEERING

LOADS CALCULATION, STRESS ANALYSIS AND BIRD STRIKE SIMULATION OF A COMPOSITE WING LEADING EDGE

VÝPOČET ZATÍŽENÍ, ANALÝZA PEVNOSTI A SIMULACE NÁRAZU PTÁKA PRO KOMPOZITNÍ NÁBĚŽNÉ HRANY KŘÍDLA

DIPLOMOVÁ PRÁCE
MASTER'S THESIS

AUTOR PRÁCE
AUTHOR
Bc. RAMAN ZUBRYTSKI

VEDOUCÍ PRÁCE
SUPERVISOR
VOLODYMYR SYMONOV, M.Sc.

BRNO 2015

Vysoké učení technické v Brně, Fakulta strojního inženýrství

Letecký ústav
Akademický rok: 2014/2015

ZADÁNÍ DIPLOMOVÉ PRÁCE

student(ka): Bc. Raman Zubrytski

který/která studuje v **magisterském navazujícím studijním programu**

obor: **Stavba letadel (2301T039)**

Ředitel ústavu Vám v souladu se zákonem č.111/1998 o vysokých školách a se Studijním a zkušebním řádem VUT v Brně určuje následující téma diplomové práce:

Výpočet zatížení, analýza pevnosti a simulace nárazu ptáka pro kompozitní náběžné hrany křídla

v anglickém jazyce:

Loads calculation, stress analysis and bird strike simulation of a composite wing leading edge

Stručná charakteristika problematiky úkolu:

Na základě daných konstrukčních koncepcí náběžné hrany křídla by měly být vybrány geometrické parametry a vrstvení laminátu pro konstrukční prvky s ohledem na dané zatěžovací případy a materiály. Nejzávažnější požadavek na konstrukci je přežít po nárazu ptáka případ zatížení "Get Home". Z tohoto důvodu, aby bylo možné odhadnout poškození konstrukce způsobené ptákem, měla by být provedena simulace nárazu ptáka.

Cíle diplomové práce:

S ohledem na uvedeny požadavky a materiály stanovte:
1. Geometrické parametry konstrukce slotu.
2. Vrstvení laminátu pro konstrukční prvky.

Seznam odborné literatury:

[1] CS-25. Certification Specifications on Large Aeroplanes, 2003.
[2] M. Chung-Yung Niu. "Aircraft structural design", 2nd edition. Hong Kong Conmilit Press Ltd. 1999. ISBN 962-7128-09-0.
[3] N.N. Churnaieva, M.G. Iefimova, V.P. Solonin. "Wing and means for improving take-off and landing characteristics of aircraft". Moscow. Moscow state technical university of civil aviation. 2000.
[4] M. Guida. „Study, Design and Testing of Structural Configurations for the bird - strike compliance of aeronautical components". A thesis submitted for the Doctoral Degree in Aerospace Structure. Department of Aerospace Engineering, University of Naples "Federico II". December 2008.
[5] S. Georgiadis, A.J. Gunnion, R.S. Thomson and B. K. Cartwright, "Bird-strike Simulation for Certification of the Boeing 787 Composite Moveable Trailing Edge", Composite Structures Journal, vol. 86, nos. 1-3, 2008, pp. 258-268. (http://www.sciencedirect.com/science/article/pii/S0263822308000883).
[6] Cheng-Ho Tho, M.R. Smith. "Accurate bird strike simulation methodology for BA609 tiltrotor". Journal of the American Helicopter Society, 12/2010; 56(1):12007-1-12007-10. DOI:10.4050/JAHS.56.012007.
[7] L.B.Lucy. „A Numerical Approach to the Testing of the Fission Hypothesis". Astronomical Journal, Vol. 82, 1977, pp.1013-20.
[8] "SIMULIA Abaqus User's manual". http://www.3ds.com/support/documentation/users-guide/.
[9] S. Heimbs. „Bird Strike Simulations on Composite Aircraft Structures". 2011 SIMULIA Customer Conference, Barcelona, Spain, May 17-19. 2011.

Vedoucí diplomové práce: Volodymyr Symonov, M.Sc.

Termín odevzdání diplomové práce je stanoven časovým plánem akademického roku 2014/2015.

V Brně, dne 19.11.2014

L.S.

doc. Ing. Jaroslav Juračka, Ph.D.	doc. Ing. Jaroslav Katolický, Ph.D.
Ředitel ústavu	Děkan fakulty

Abstrakt

Tato diplomová práce se zaměřuje na stanovení geometrických a materiálových parametrů konstrukce slotu letadla B737-200. V této práci je vypracovaný návrh kompozitového slotu s ohledem na dané zatěžovací případy, včetně tzv. “bird strike”. Analytické výpočty jsou ověřené metodou konečných prvků (MKP) v programech MSC.Nastran/Patran, MSC.Dytran.

Klíčová slova
konstrukce slotu, MKP, kompozitní materiál, bird strike

Abstract

This thesis deals with design of slat geometrical and material parameters of the B737-200 aircraft. In this thesis there is created design of the composite slat with respect to a given load cases including bird strike. Analytical calculations are verified by FE analysis in MSC.Nastran/Patran, MSC.Dytran software.

K**eywords**
slat construction, FEM, composite material, bird strike

Bibliographic citation

ZUBRYTSKI, R. *Loads calculation, stress analysis and bird strike simulation of a composite wing leading edge.* Brno: Brno University of Technology, Faculty of mechanical engineering, 2015. 59 p. Supervised by Volodymyr Symonov, M.Sc.

Declaration of authenticity

I declare that I have elaborated my master thesis on the theme of "Loads calculation, stress analysis and bird strike simulation of a composite wing leading edge" independently, under the supervision of the master's thesis supervisor and with the use of technical literature and other sources of information which are all quoted in the thesis and detailed in the list of literature at the end of the thesis.

In Brno 05.06.15 .....

Raman Zubrytski

Acknowledgements

On the first place I would like to express my gratitude to my parents who were supporting me during whole my study period.

This way I would also like to thank my master thesis supervisor Volodymyr Symonov, M.Sc., for his continuing support, guidance, patient and valuable tips during this challenging thesis.

TABLE OF CONTENTS

1. Introduction 9
1.1 CS-25 Bird Strike Requirements [2] 9
2 Material model 11
2.1 Material models description 11
2.1.1 MAT8 material model 11
2.1.2 MAT54 material model 11
2.1.3 MAT58 material model 11
2.2 Numerical simulations 12
2.2.1 LS-DYNA MAT58 material model 12
2.2.2 LS-DYNA MAT8 material model 18
2.3 Material models comparison 22
2.4 Material model choosing 23
3 Slat construction 25
3.1 Slat concept 25
3.2 Airplane prototype 25
3.3 Slat location 26
3.4 Slat geometry 27
3.4.1 CAD model 27
3.5 Slat attachment position 28
3.6 Material 28
3.7 Slat loads 29
3.7.1 Analytical loadings calculation 29
3.8 Slat thickness calculation 32
3.8.1 Calculation methodology 32
3.8.2 Calculation algorithm 35
3.8.3 Calculation results 35
3.9 FE stress analysis of the slat 36
3.9.1 FE model description 36
3.9.2 Slat FE simulation 37
3.10 Wing deflection influence 39
3.11 Slat construction recalculation 41
3.12 Slat construction summary 41
4 Bird strike simulation 42
4.1 Bird modelling 42

4.2 Bird modelling methods 43
4.2.1 Lagrangian modelling 43
4.2.2 Eulerian modelling 43
4.2.3 Arbitrary Lagrangian Eulerian (ALE) modelling 44
4.2.4 Smoothed Particle Hydrodynamics (SPH) modelling 45
4.3 Bird-strike simulation in MSC.Dytran software 46
4.3.1 Simulation conditions 46
4.3.2 Simulation results 47
4.4 Simulation results assessment 50
5 Conclusion 51
6 Bibliography 52
7 List of figures 54
8 List of tables 56
9 Appendix 57

1. Introduction

Composite structures are increasingly being used within the aircraft industry, even for primary structures. Same time, the application of composites within impact-endangered areas is very limited.

Collision of airplanes and birds presents a potentially hazardous situation, which is becoming much more frequent due to the ever-increasing air traffic and changes in the migration routes of bird flocks [1]. Compared to metallic structures, energy absorption and damage mechanisms of composite materials are far more complex and depend on a number of parameters such as fiber and matrix properties, ply layup, total number of layers, interfacial properties and bonding strength, impactor geometry, impact velocity and impactor initial energy. Difficulty is that high performance composites only can afford plastic strain of about 2-3% while recent aluminum alloys around 20%.

Aircraft leading edges must be certified for a proven level of bird impact resistance. In particular, the main structural requirement is to protect the torsion box and control devices from any significant damage caused by bird strike in order to allow the aircraft to land safely. In more details, certification requirements are shown in chapter 1.1.

The primary subject of the **present paper** is to develop a typical large transport airplane **flap structure** composite slat and it damage assessment according to certification requirements.

1.1 CS-25 Bird Strike Requirements [2]

CS 25.631 requires that the aeroplane must be designed to assure capability of continued safe flight and landing of the aeroplane after impact with a 4 lbs bird when the velocity of the aeroplane (relative to the bird along the aeroplane's flight path) is equal to Vc at sea-level or 0.85 Vc at 8000 ft, whichever is the more critical. The phrase “continued safe flight and landing” in this respect may be interpreted in different ways and the effects of bird strike are addressed in various other sections of CS-25:

- (a) CS 25.571(e) which requires that the aeroplane must be capable of successfully completing a flight during which likely structural damage occurs as a result of bird impact as specified in CS 25.631. The AMC to 25.571 (in paragraph 2.7.2) specifies the loads associated with “get home” conditions that have to be met for this case;
- (f) AMC 25.1309(b) where bird strike is identified as a Particular Risk requiring investigation as part of the Common Cause Analysis.

(1)Initially all areas/zones of the aircraft prone to bird strike should be considered, either pressurized or non-pressurized, either primary or secondary structure. This would normally include areas/zones such as:

- (g) Wings (leading edges (including slats), trailing edges (flaps));

For high lift devices (flaps and slats) instead of using Vc at sea-level or 0.85 Vc at 8000 ft, the appropriate maximum design speed (as per CS 25.335(e)) may be taken as the basis for determining the bird impact damage. For landing gears, the appropriate maximum speed (asper CS 25.1515) may be taken as the basis for determining the bird impact damage.

(2)Showing that under the conditions of CS 25.631 no bird penetration and no part loss occurs in the aircraft areas/zones where bird strike is of concern, is the preferred certification approach. For this scenario, continued safe flight and landing should be further substantiated considering the following effects:

- (a) Bird-strike induced deformation of structures on internal structural items, such as instrument panels or avionics racks;
- (b) Bird-strike induced deformation of structures on underlying items, systems and equipment, or on operational approved performance (corrective pilot action may be considered);and
- (c) Bird-strike induced accelerations on items, systems and equipment.

(3) If contrary to item (2) above, bird penetration and/or part loss does occur in the aircraft areas/zones where bird strike is of concern, the following should be considered:

- (a) The effects of subsequent impacts on items, systems and equipment after penetration should not prohibit continued safe flight and landing;
- (f) For bird penetration into the fuel tanks (e.g. through wing leading edge and front spar)
  it must be substantiated that fire or other hazards (e.g. the resulting fuel imbalance or the inability to continue the normal flight) would not preclude continued safe flight and landing. Fuel tank leaks due to bird strike in the vicinity or upstream path of heat sources (landing gears, engines) would normally not be considered acceptable;
- (g) The effects on continued safe flight and landing of damage and subsequent release of debris resulting from bird impact should also be addressed, for example for flaps, landing gear doors and large antennas. The effects of such parts loss should not prohibit continued safe flight and landing. This evaluation should include the effect of any debris impacting other parts of the aircraft (e.g. empennage area or engines) and should consider any hazardous asymmetric conditions arising. The use of design features such as multiple attachment points, the application of engineering judgement and the review of relevant service experience may be used to support this evaluation.

2 Material model

2.1 Material models description

There are numbers of finite element (FE) codes used to predict the dynamic damage of composite materials, such as LS-DYNA, ABAQUS Explicit, RADIOSS, and PAM-CRASH, which use composite material models to define the elastic, failure, and post-failure behavior of the elements. These material models account for physical properties of the material that can be measured by experiment (such as strength, modulus, and strain-to-failure) but also include software specific parameters, which either have no physical meaning or cannot be determined experimentally. Usage of non-physical parameters thus requires extensive calibration and tweaking of these material models in order to reach an agreement between experiment and simulation [3].

There are a bunch of material models such as MAT22, MAT54, and MAT55 (use a ply discount method to degrade elastic material properties), MAT58, MAT158, and MAT162 (use continuum damage mechanics to degrade the elastic properties after failure), MAT8 are available. For future comparison have been chosen MAT8, MAT54, and MAT58. Short description of each is shown below.

2.1.1 MAT8 material model

MAT8 (MSC.NASTRAN Orthotropic Elastic) material model is used for describing the elasticity characteristics of an anisotropic material, assuming linear orthotropic behavior. The accuracy of this model depends on the assumption that it will stay within the bounds of the linear portion of the stress-strain curve. This model represents a suitable approximation to modeling thin anisotropic parts such as fiber-filled injection molded products/components [4].

2.1.2 MAT54 material model

The LS-DYNA MAT54 material model is of interest for large full-scale structural damage simulations because it is a relatively simple material model with minimal input parameters. Not only does this reduce the computational requirement of a simulation, it also reduces the difficulty and amount of material testing necessary to generate the input parameters [3].

2.1.3 MAT58 material model

MAT58 material model is so called elastic damage model, where it is assumed that the deformation introduces micro cracks and cavities into the material. These defects cause primarily stiffness degradation with rather small permanent deformations unless the material undergoes rather high loading and is not close to deterioration. The main difference to MAT54 material model lies in the smooth increase of damage; no sudden change of material behavior occurs which appears more correct [5] [6].

2.2 Numerical simulations

Chosen material models (MAT8, MAT58) behavior were simulated in Dytran software and compared to each other and to the MAT54 material model. The main criteria for the models comparison was the minimum mistake in elastic and strength properties and elastic energy in relation to the experimental data. The assessment of the LS-DYNA MAT54 material model was done by M. Osborne in [3] using the same criteria. There was used Toray T700GC-12K-31E/#2510 [3] unidirectional (UD) carbon-epoxy tape which properties are shown below in Tab. 1. Experimental tests included uniaxial tension and compression specimens about the two material axes. Simulations were done by methodology presented in [3]. The current assessment is aimed to comparison of MAT8, MAT58 simulation to MAT54 behavior studies and experimental tests.

Matl. Dir.	Property	Units	Tension			Compression		
			AGATE	MIL-HDBK-17	DYNA	AGATE	MIL-HDBK-17	DYNA
1/ Fiber	Strength	ksi	314	319	319	210	213	213
	Modulus	Msi	18.1	18.4	18.4	16.3	16.5	18.4
	Strain	u in/in	17,366	17,337	17,400	12,846	12,909	11,600
2/ Matrix	Strength	ksi	7.09	7.09	7.09	28.8	28.8	28.8
	Modulus	Msi	1.22	1.22	1.22	1.22	1.47	1.22
	Strain	u in/in	5,813	5,811	24,000	23,618	19,592	24,000

Table 1 Toray T700GC-12K-31E/#2510 UD Tape Properties

2.2.1 LS-DYNA MAT58 material model

Stress-strain and energy-strain curves were taken from tests data [3] for L (longitudinal), T (transverse), and CP (±45° cross-ply) case.

2.2.1.1 Simulation conditions

All laminates were defined using the "Shell laminate properties" menu input card, which accepted material, thickness, and orientation (angle) on a ply-by-ply basis. The Nastran CQUAD4 shell element was used for all simulations. Each laminate was subjected to tension and compression along perpendicular loading axes (i.e. longitudinal and transverse). Rather than modifying either the element connectivity or applied loading, transverse loading was accomplished by rotating a laminate's plies by 90 degrees. In addition to the longitudinal and transverse boundary conditions shown in Figure 1, all out-of-plane displacements were constrained (Z-axis in the global Coordinate System (CS)).

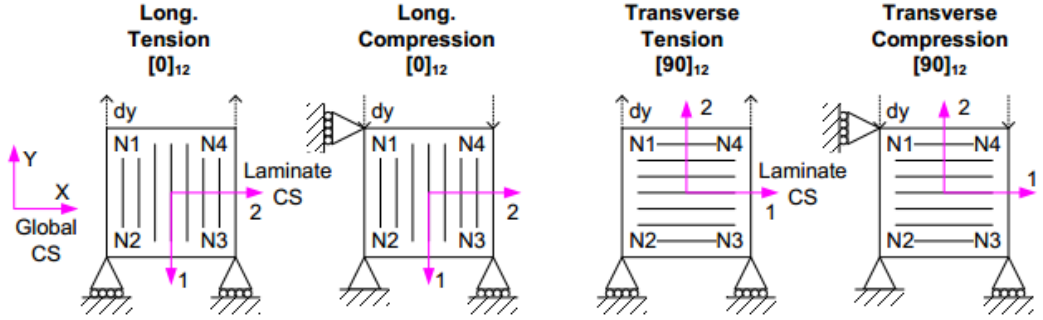

Figure 1 Single Element Mesh, Boundary Conditions, & Loading

The cross-ply simulations began with the input deck from the UD simulations of the first section. This included the MAT58 material model, loading, boundary conditions, and element geometry. The primary difference for the 12-ply cross-ply laminate was the individual ply-orientations. The loading and boundary conditions are shown on Figure 2; compressive simulations required off-axis (lateral) supports to prevent unconstrained lateral displacement.

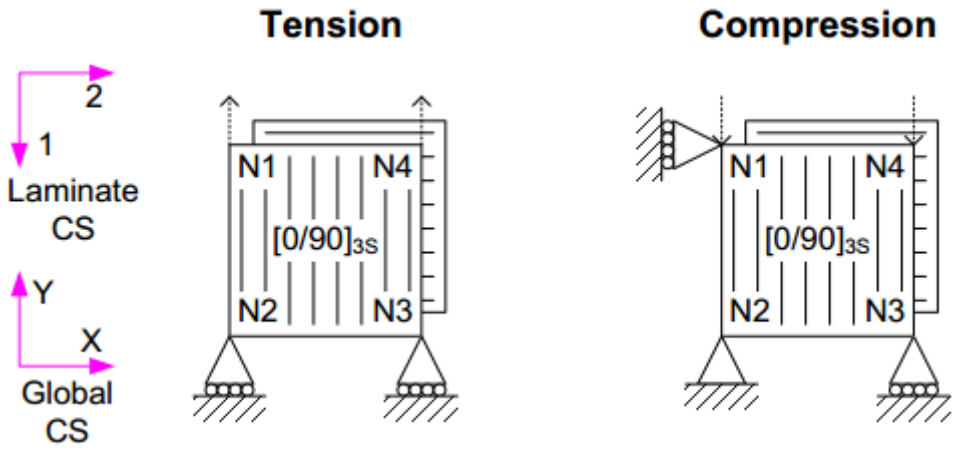

Figure 2 Cross-Ply Simulations – Loading and Boundary Conditions

2.2.1.2 Results

In order to get the least possible difference between experimental tests and simulations material (elastic modulus, shear modulus, ultimate failure, etc.) and special parameters (element deleting time step, max. effective strain for failure, etc.) have been selected.

Results from the $[0]_{12}$, $[90]_{12}$ and cross-ply coupon tests.

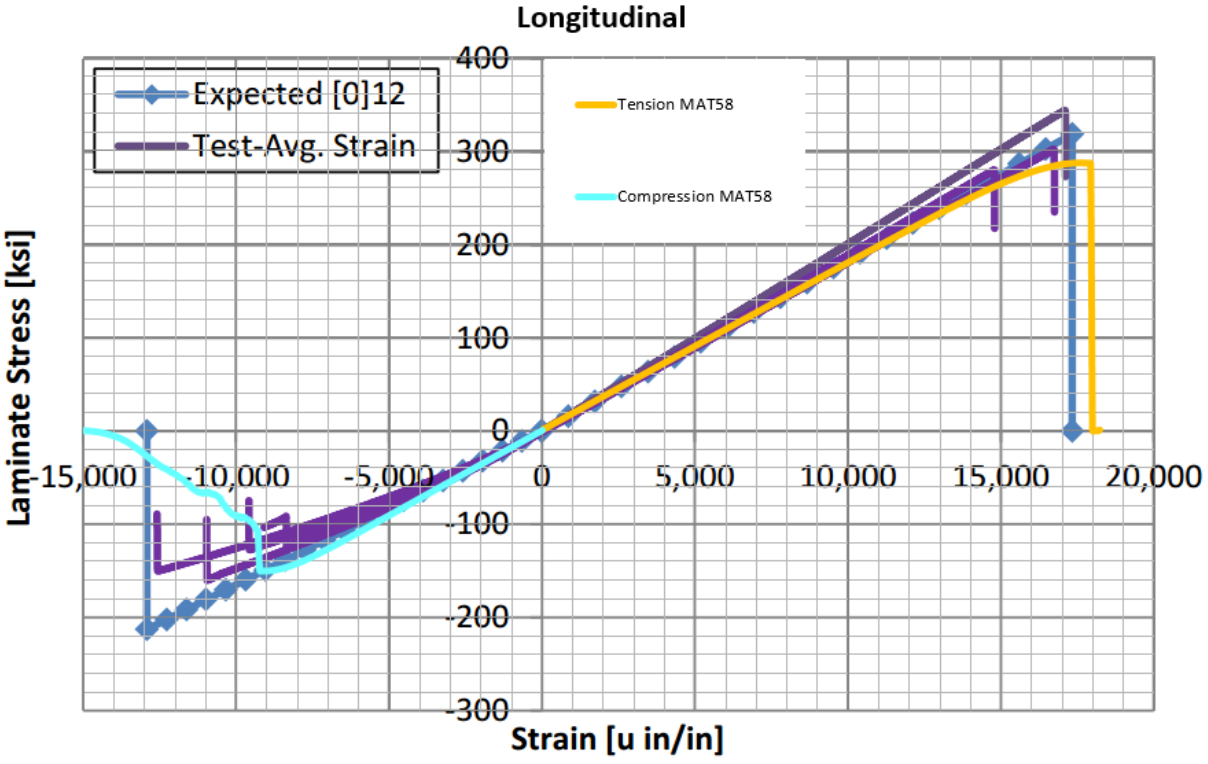

Figure 3 Stress vs. Strain – MAT58, longitudinal

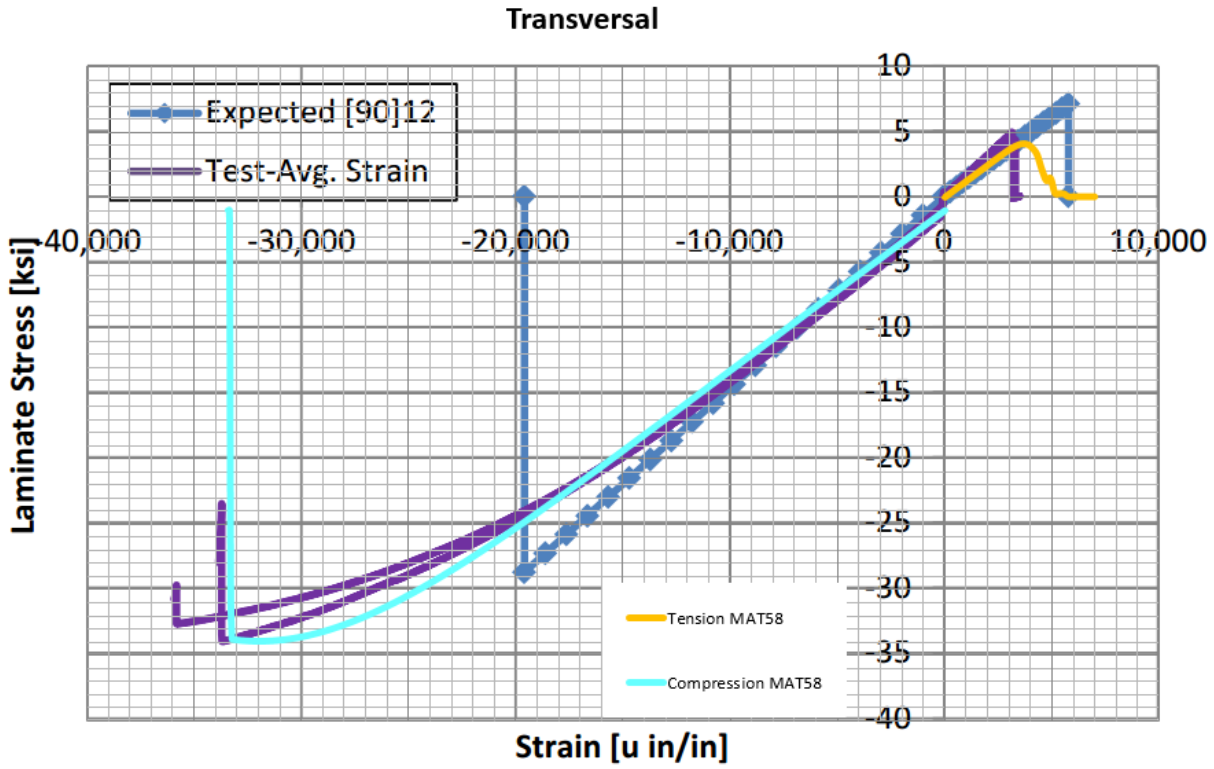

Figure 4 Stress vs. Strain – MAT58, transversal

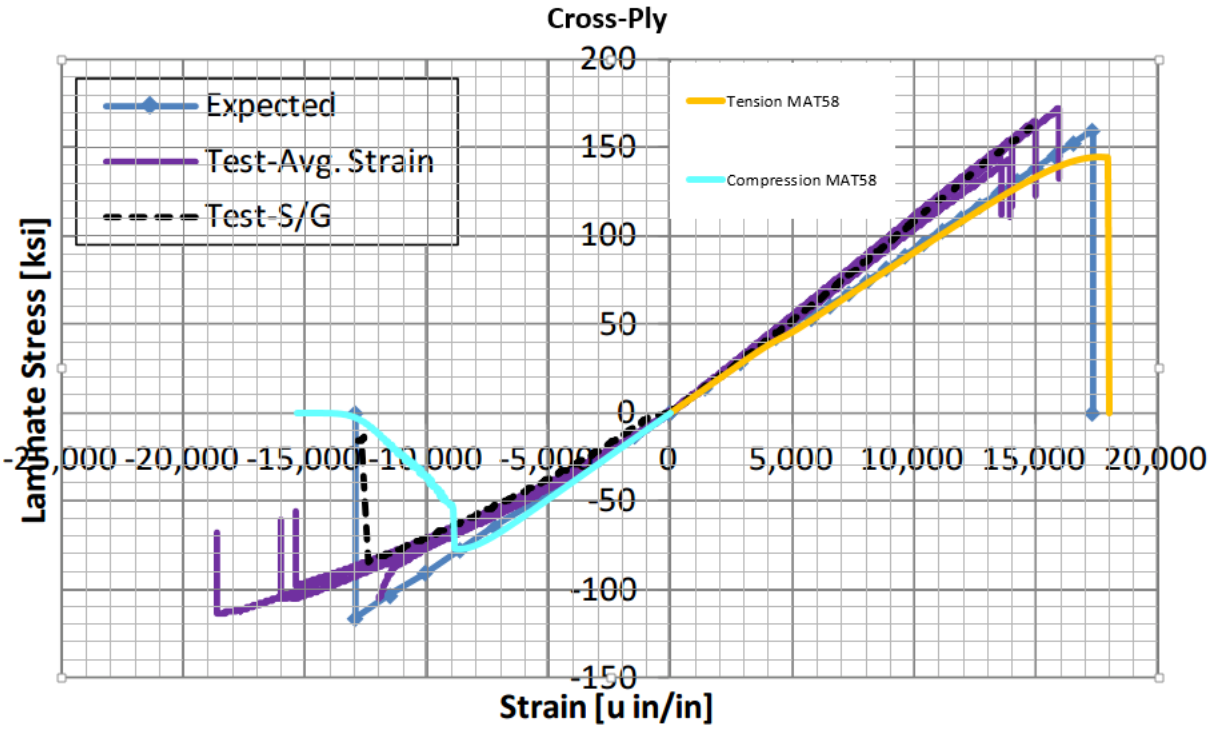

Figure 5 Stress vs. Strain – MAT58, cross-ply

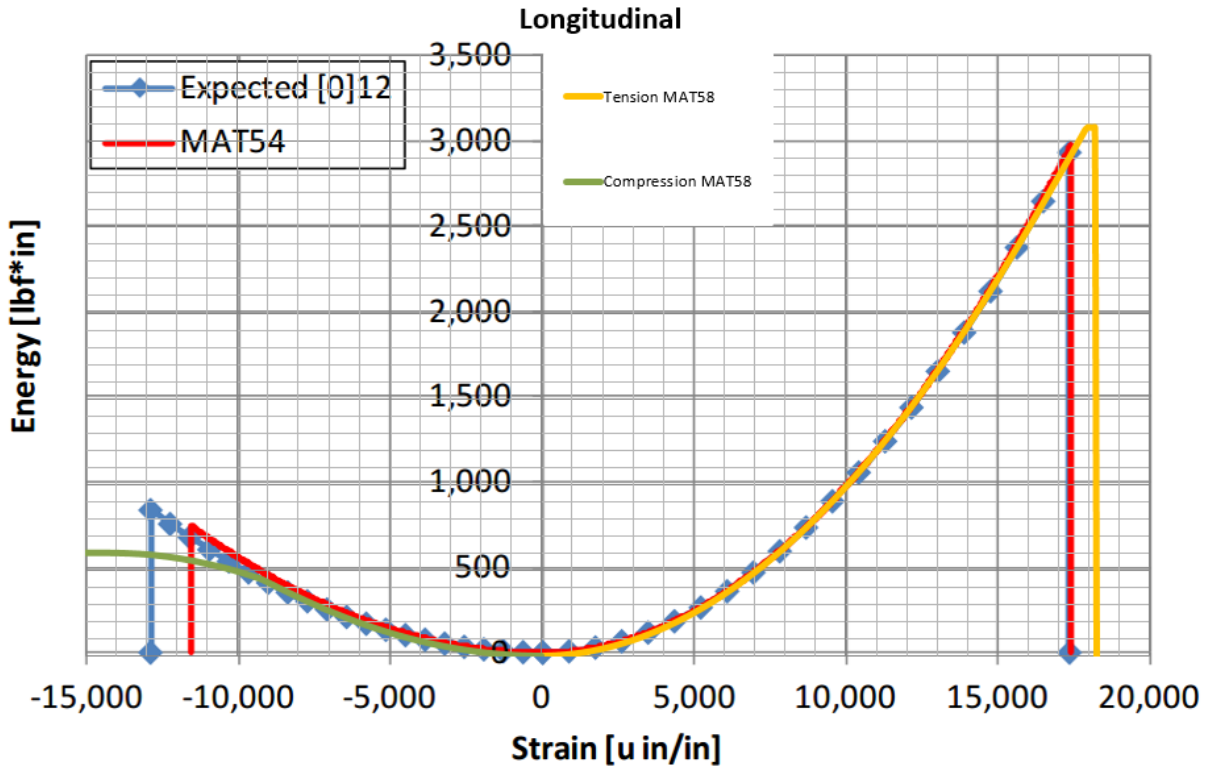

Figure 6 Energy vs. Strain – MAT58, longitudinal

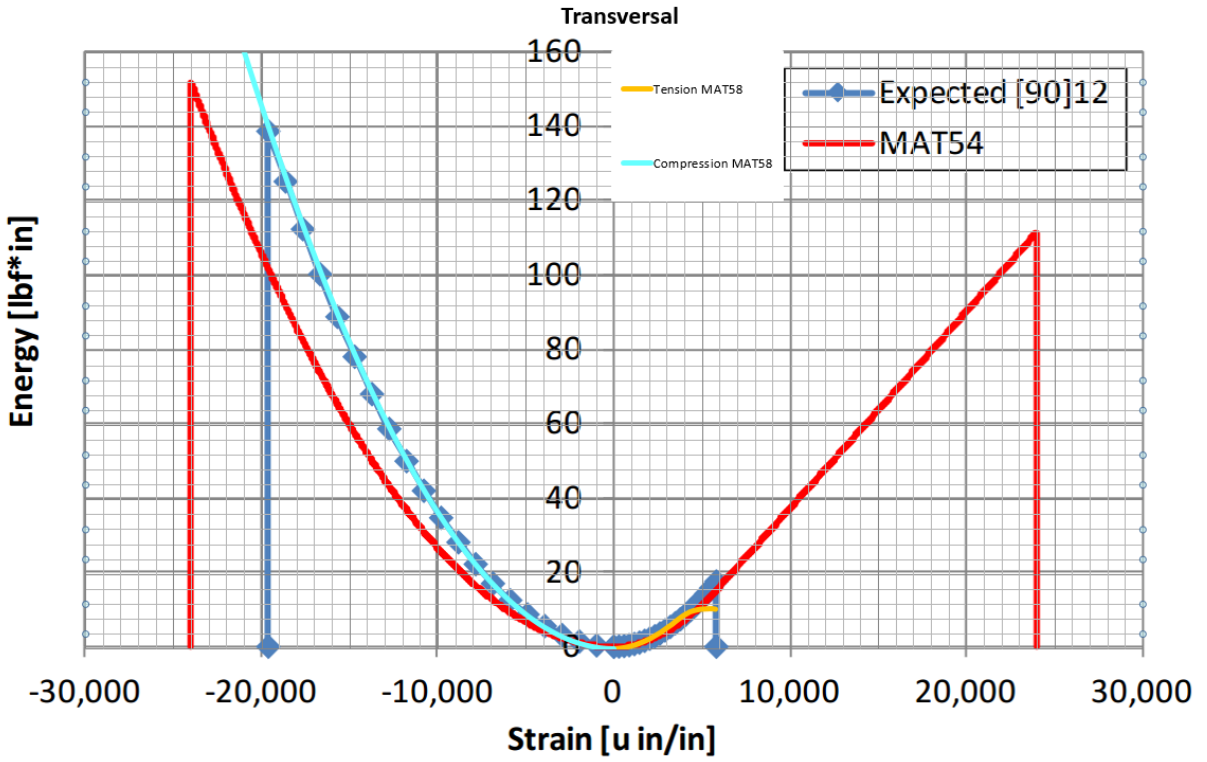

Figure 7 Energy vs. Strain – MAT58, transversal

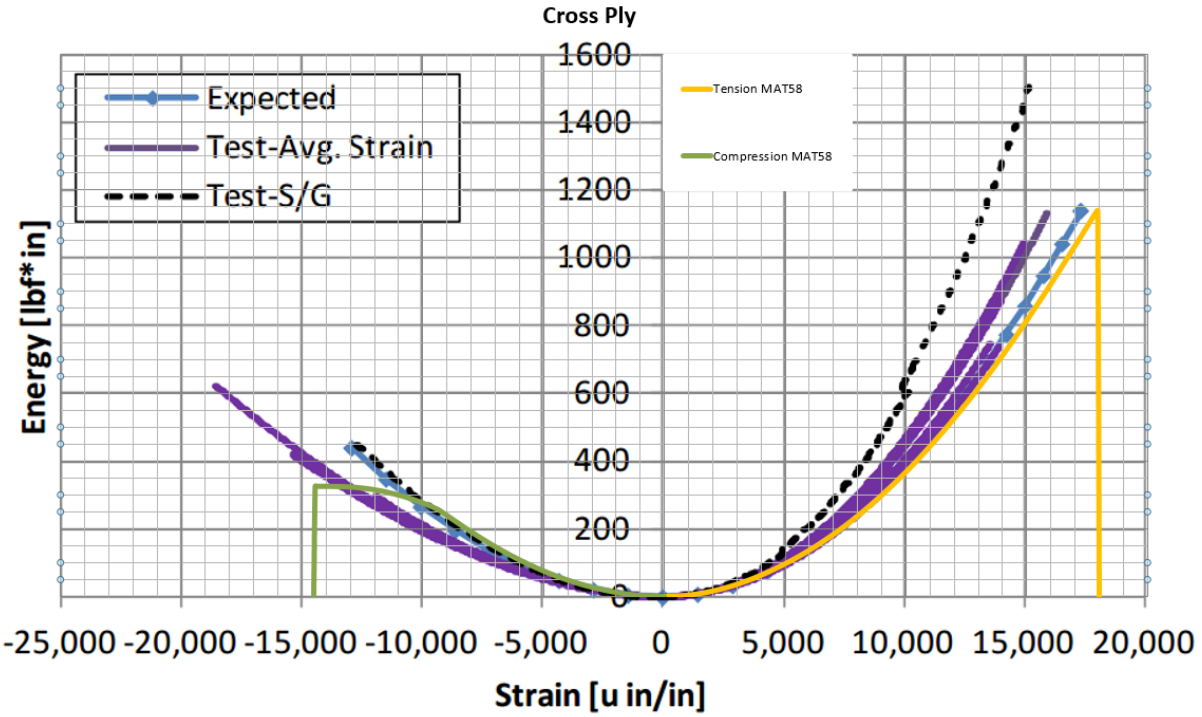

Figure 8 Energy vs. Strain – MAT58, cross-ply

Tables 2, 3, 4 provide comparison of elastic modulus, failure strength, and peak energy between the experimental, theoretical (expected) and MAT58 results.

Loading	Quantity	Modulus[Msi]	Strength[ksi]	Energy[lbf*in]
Tension	Expected	18.1	314	2929
	MAT58	18.10	287.17	3080.28
	Error	0%	-9%	5%
	Test	18.84	309.8	2664
	MAT58	18.10	287.17	3080.28
	Error	-4%	-7%	16%
Compression	Expected	16.5	-213	834
	MAT58	18.10	-150.11	602.31
	Error	10%	-30%	-28%
	Test	16.29	-143	492
	MAT58	18.10	-150.11	602.31
	Error	11%	5%	22%

Table 2 UD $[0]_{12}$ results - MAT58

Loading	Quantity	Modulus[Msi]	Strength[ksi]	Energy[lbf*in]
Tension	Expected	1.22	7.1	18
	MAT58	1.22	4.06	10.93
	Error	0%	-43%	-39%
	Test	1.36	4.5	5
	MAT58	1.22	4.06	10.93
	Error	-10%	-10%	119%
Compression	Expected	1.47	-29	139
	MAT58	1.22	-33.00	381.92
	Error	-17%	14%	175%
	Test	1.57	-33	318
	MAT58	1.22	-33.00	381.92
	Error	-22%	0%	20%

Table 3 UD $[90]_{12}$ results - MAT58

Loading	Quantity	Modulus[Msi]	Strength[ksi]	Energy[lbf*in]
Tension	Expected	9.81	160	1140
	MAT58	9.66	144.40	1138.15
	Error	-2%	-10%	0%
	Test	10.58	157	1008
	MAT58	9.66	144.40	1138.15
	Error	-9%	-8%	13%
Compression	Expected	8.99	-116	441
	MAT58	9.66	-80.99	326.57
	Error	7%	-30%	-26%
	Test	8.84	-102	509
	MAT58	9.66	-80.99	326.57
	Error	9%	-21%	-36%

Table 4 Cross-ply results - MAT58

2.2.2 LS-DYNA MAT8 material model

Used simulation methods are the same as for MAT58 material model, so that boundary conditions and load are the same too.

2.2.2.1 Results

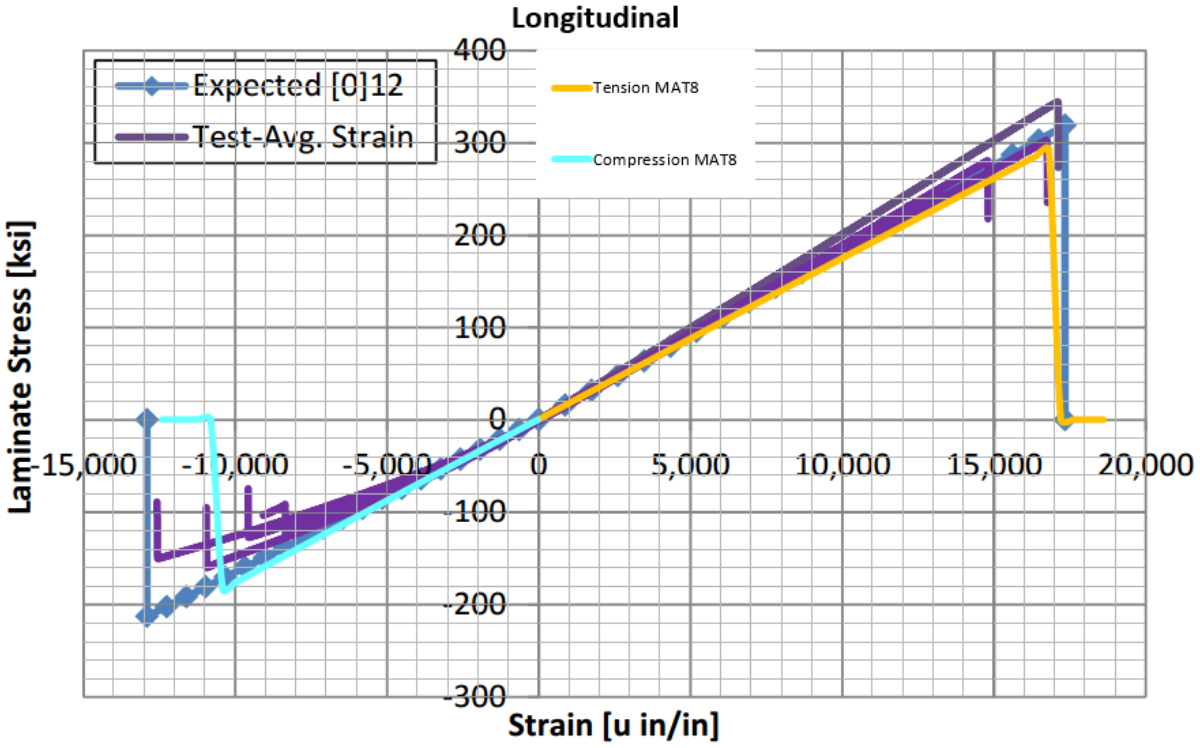

Figure 9 Stress vs. Strain – MAT8, longitudinal

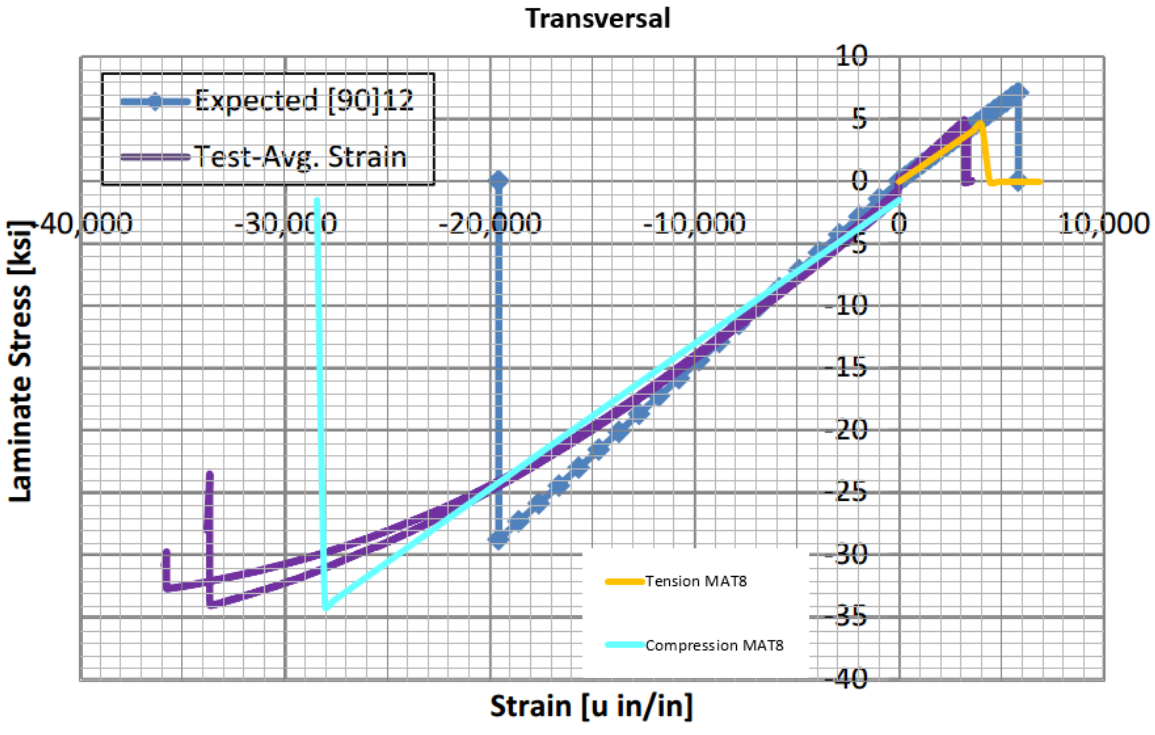

Figure 10 Stress vs. Strain – MAT8, transversal

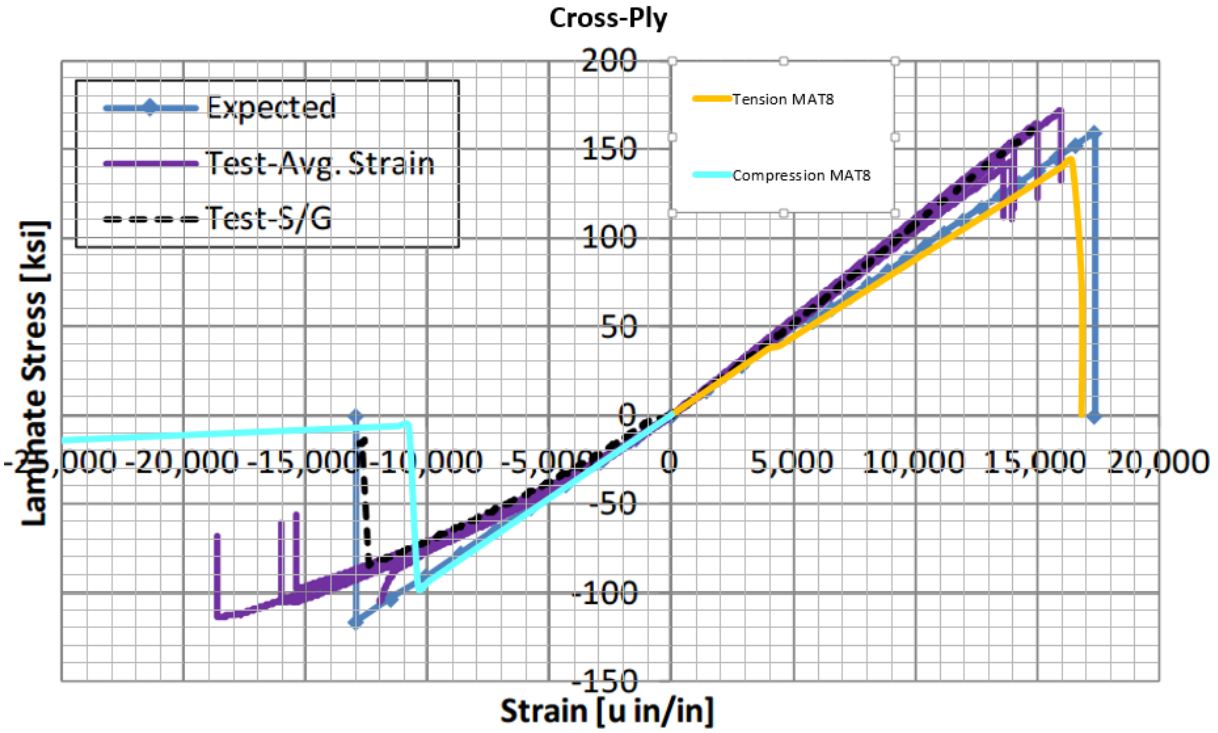

Figure 11 Stress vs. Strain – MAT8, cross-ply

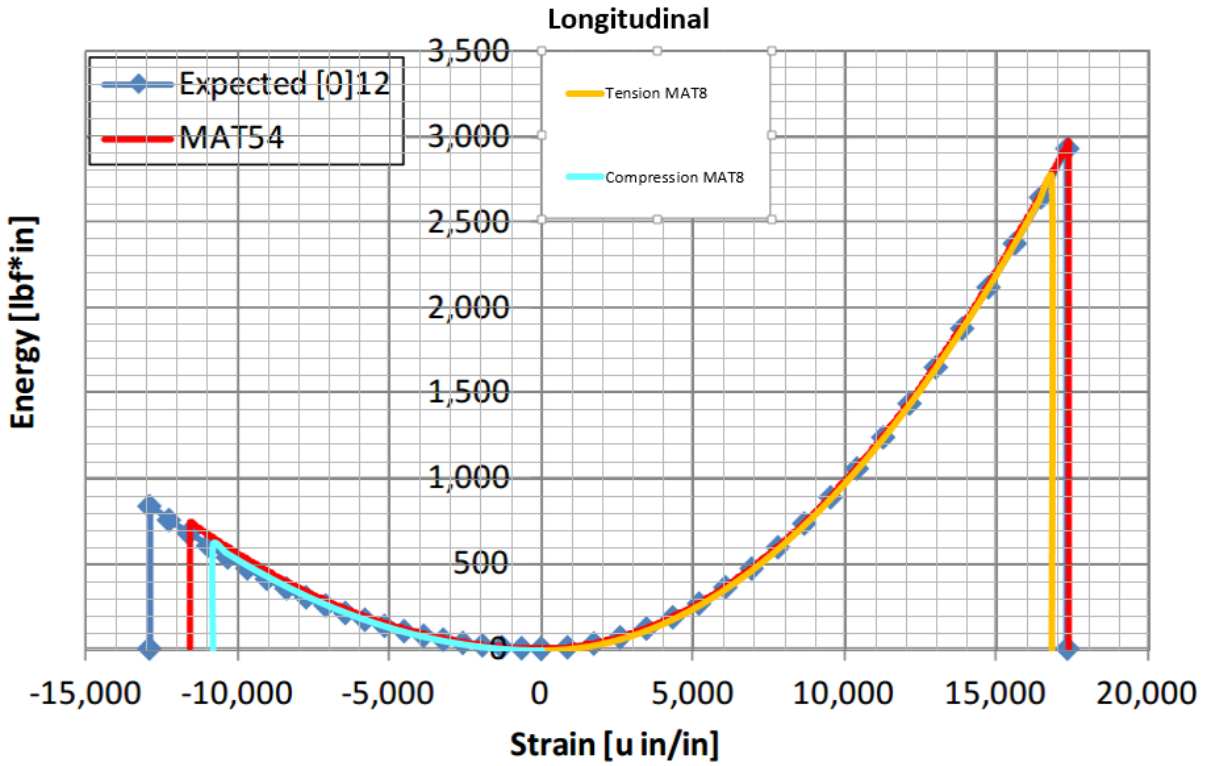

Figure 12 Energy vs. Strain – MAT8, longitudinal

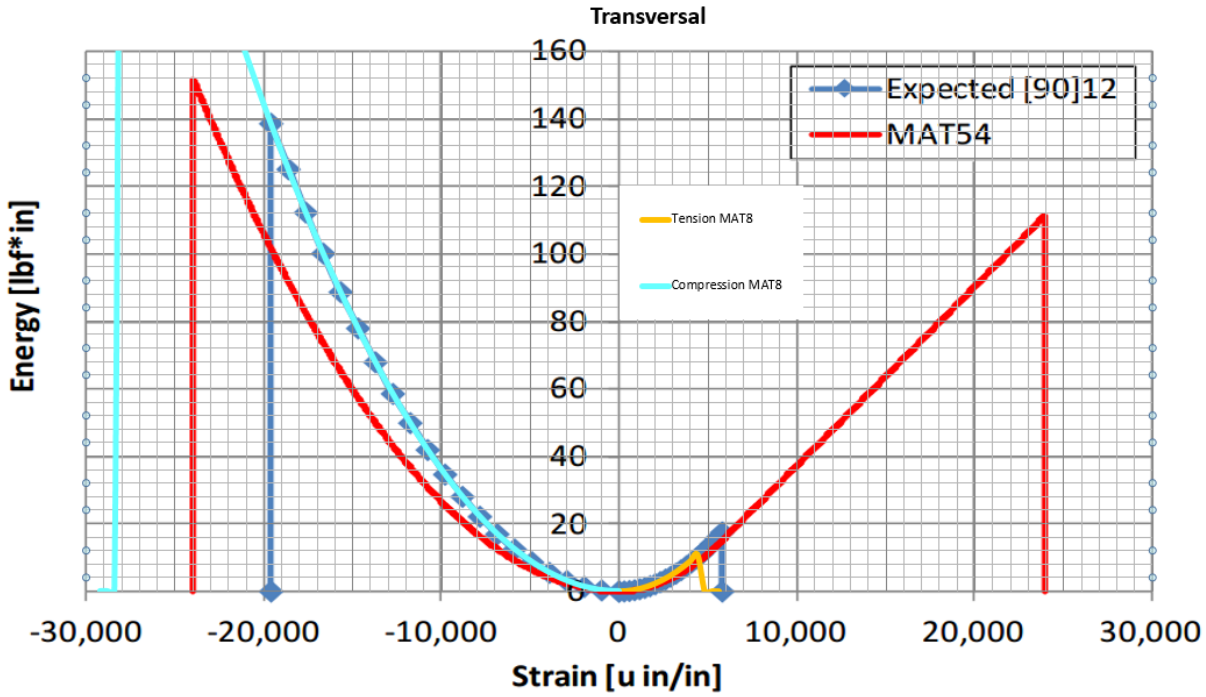

Figure 13 Energy vs. Strain – MAT8, transversal

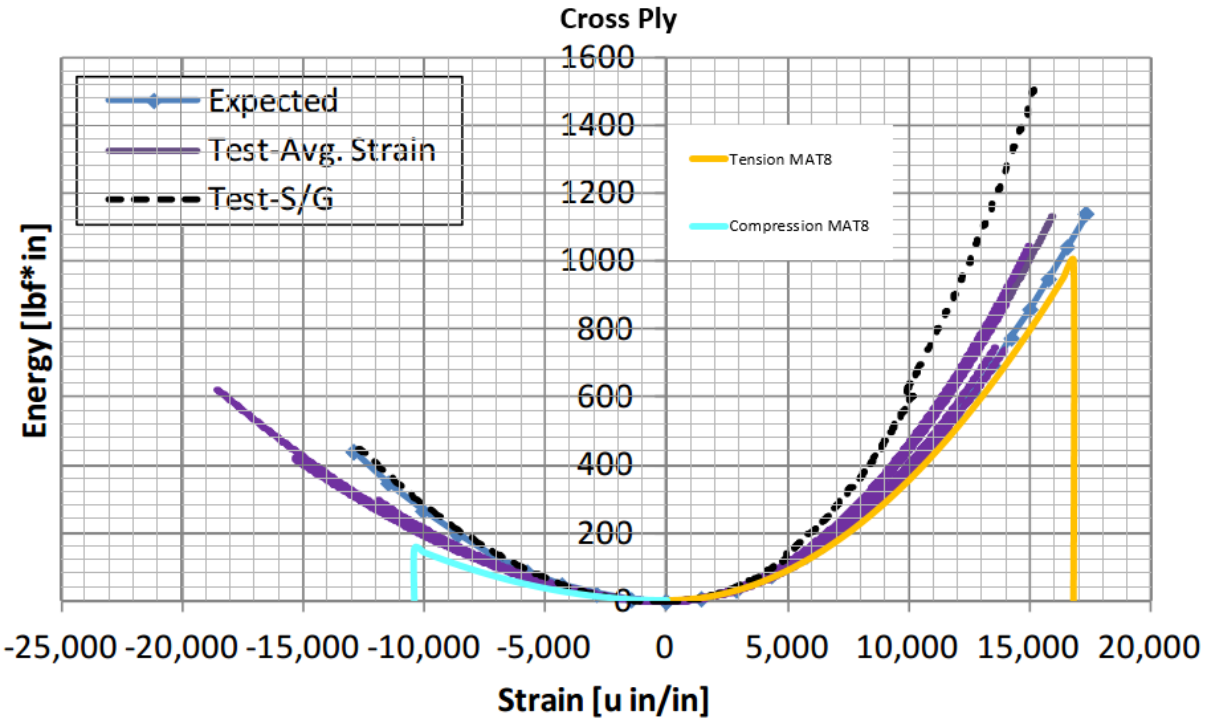

Figure 14 Energy vs. Strain – MAT8, cross-ply

Tables 5, 6, 7 provide comparison of elastic modulus, failure strength, and peak energy between the experimental, theoretical (expected) and MAT8 results.

Loading	Quantity	Modulus[Msi]	Strength[ksi]	Energy[lbf*in]
Tension	Expected	18.1	314	2929
	MAT8	17.55	292.66	2759.91
	Error	-3%	-7%	-6%
	Test	18.84	309.8	2664
	MAT8	17.55	292.66	2759.91
	Error	-7%	-6%	3%
Compression	Expected	16.5	-213	834
	MAT8	17.55	-183.63	619.85
	Error	6%	-16%	-35%
	Test	16.29	-143	492
	MAT8	17.55	-183.63	619.85
	Error	7%	22%	21%

Table 5 UD $[0]_{12}$ results - MAT8

Loading	Quantity	Modulus[Msi]	Strength[ksi]	Energy[lbf*in]
Tension	Expected	1.22	7.1	18
	MAT8	1.15	4.58	10.85
	Error	-6%	-55%	-66%
	Test	1.36	4.5	5
	MAT8	1.15	4.58	10.85
	Error	-19%	2%	54%
Compression	Expected	1.47	-29	139
	MAT8	1.15	-32.54	282.97
	Error	-28%	11%	51%
	Test	1.57	-33	318
	MAT8	1.15	-32.54	282.97
	Error	-37%	-1%	-12%

Table 6 UD $[90]_{12}$ results - MAT8

Loading	Quantity	Modulus[Msi]	Strength[ksi]	Energy[lbf*in]
Tension	Expected	9.81	160	1140
	MAT8	9.35	143.51	999.32
	Error	-5%	-11%	-14%
	Test	10.58	157	1008
	MAT8	9.35	143.51	999.32
	Error	-13%	-9%	-1%
Compression	Expected	8.99	-116	441
	MAT8	9.35	-98.28	151.52
	Error	4%	-18%	-191%
	Test	8.84	-102	509
	MAT8	9.35	-98.28	151.52
	Error	5%	-4%	-236%

Table 7 Cross-ply results - MAT58

2.3 Material models comparison

Comparison is based on an assessment of a summary of errors in longitudinal, transversal directions, and cross-ply case in relation to the experimental data. Results are shown below in tables 8-12.

Loading	Quantity	Strength[ksi]	Energy[lbf*in]
Tension	MAT54	3%	11%
	MAT58	7.30%	15.63%
	MAT8	5.53%	2.29%
Compression	MAT54	49%	51%
	MAT58	4.97%	22.42%
	MAT8	8.59%	9.76%

Table 8 Summary of errors – longitudinal

Loading	Quantity	Strength[ksi]	Energy[lbf*in]
Tension	MAT54	57%	220%
	MAT58	9.76%	118.61%
	MAT8	1.69%	73.12%
Compression	MAT54	79%	50%
	MAT58	0.01%	20.10%
	MAT8	1.38%	14.44%

Table 9 Summary of errors – transversal

Loading	Quantity	Strength[ksi]	Energy[lbf*in]
Tension	MAT54	2%	11%
	MAT58	8.73%	11.44%
	MAT8	8.61%	3.78%
Compression	MAT54	4%	4%
	MAT58	25.94%	55.86%
	MAT8	18.57%	53.28%

Table 10 Summary of errors – cross ply

Loading	Quantity	Strength[ksi]	Energy[lbf*in]
Tension	MAT54	21%	81%
	MAT58	8.60%	48.56%
	MAT8	5.28%	26.40%
Compression	MAT54	44%	35%
	MAT58	10.31%	32.79%
	MAT8	9.51%	25.83%

Table 11 Summary of errors – mean

Quantity	Strength[ksi]	Energy[lbf*in]
MAT54	32%	58%
MAT58	9.45%	40.68%
MAT8	7.39%	26.11%

Table 12 Summary of errors – final

2.4 Material model choosing

Final error was calculated as average value from tension and compression (longitudinal, transversal, cross-ply). As shown on Figure 15 the least computational error has MAT8 material model, so that it was chosen for further bird strike simulation.

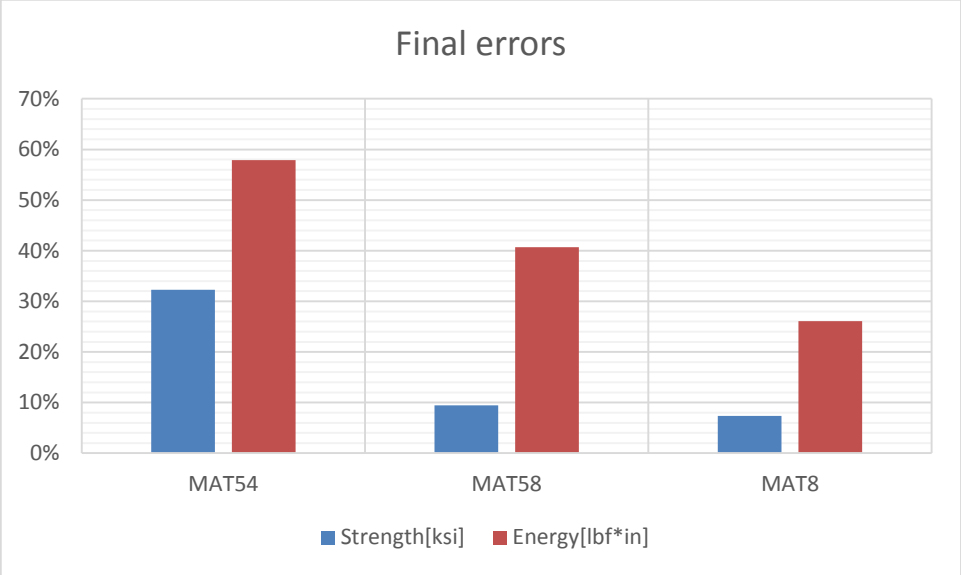

Figure 15 Final errors – comparison

MAT8 is simpler than MAT58 material model, which is the main advantage of this model. However, this material model can only simulate linear shear stress-strain curve, which is the main disadvantage in comparison to MAT58 material model. Behavior of these models at shear loading is shown below.

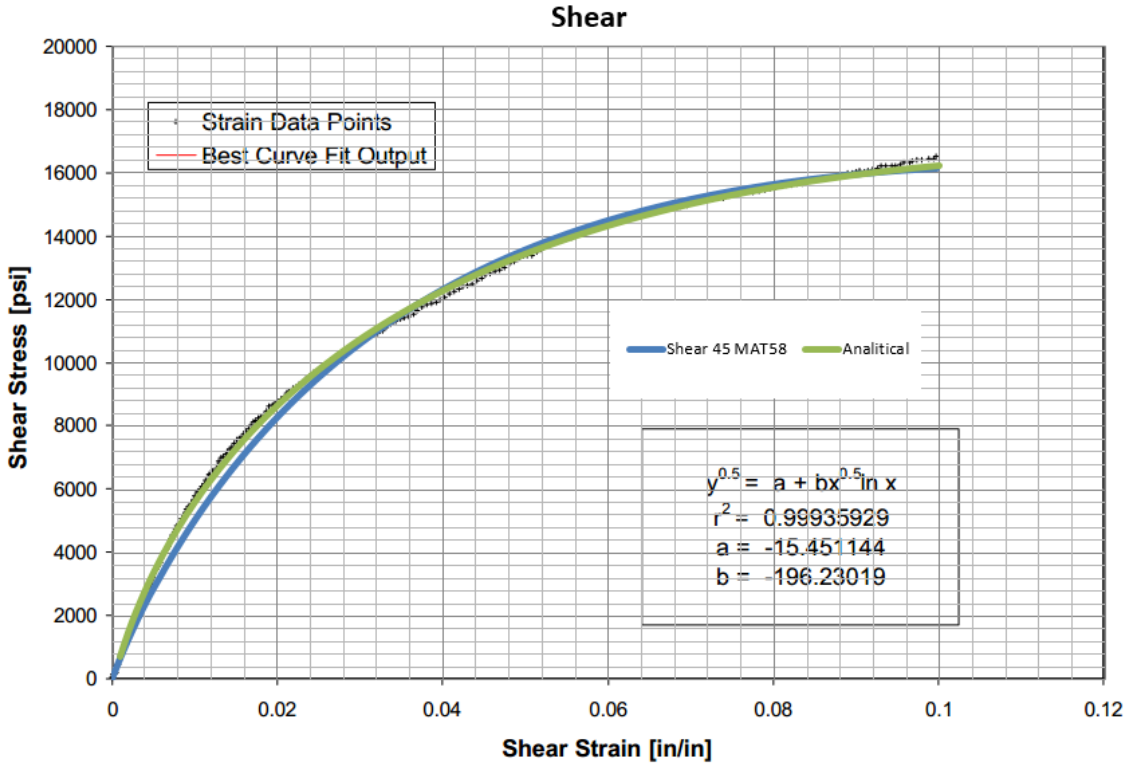

Figure 16 Stress vs. Strain – MAT58, tensile test of a ±45° laminate

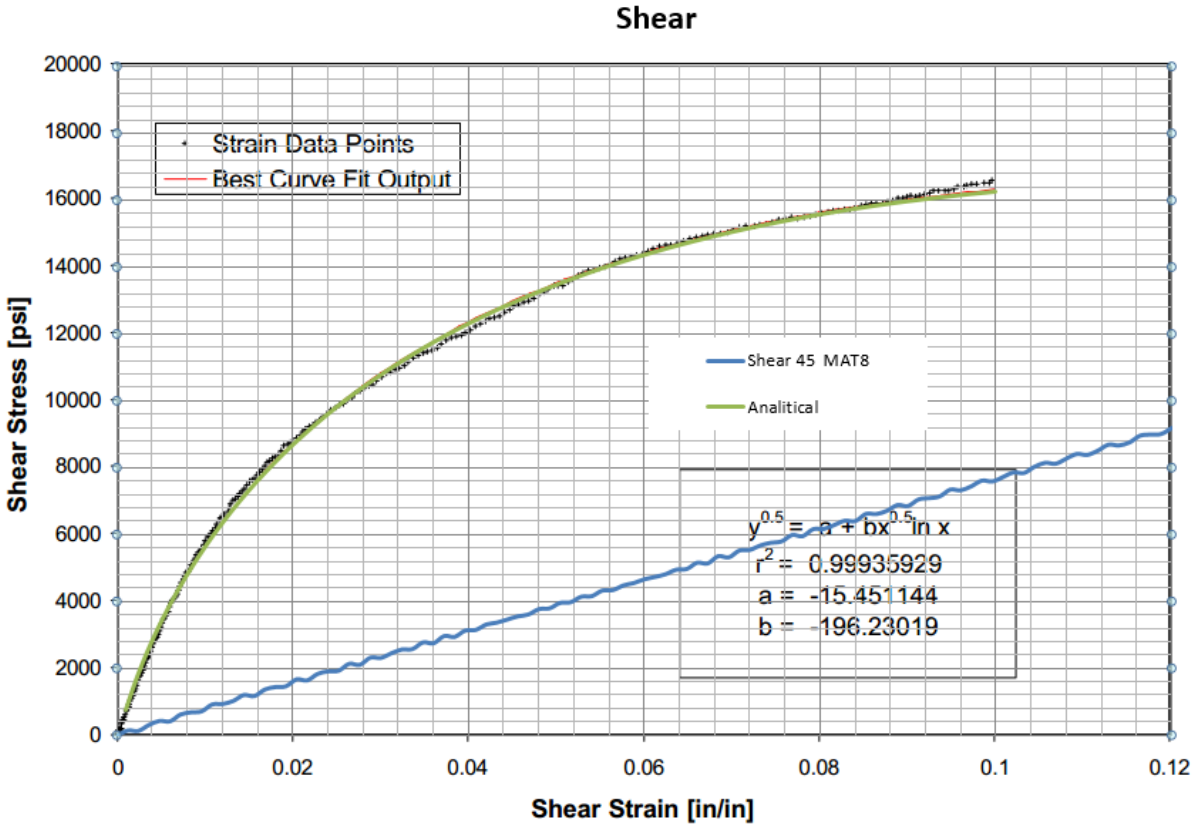

Figure 17 Stress vs. Strain – MAT8, tensile test of a ±45° laminate

3 Slat construction

Slats are aerodynamic surfaces on the leading edge of the wings which, when deployed, allow the wing to operate at a higher angle of attack. A higher coefficient of lift is produced as a result of angle of attack and speed, so by deploying slats an aircraft can fly at slower speeds, or take off and land in shorter distances. They are usually used while landing or performing maneuvers which take the aircraft close to the stall, but are usually retracted in normal flight to minimize drag.

3.1 Slat concept

In order to make an efficient slat it is needed to count mutual influences of several factors, such as manufacturing, impact performance, weight and costs. According to [7] there are number of concepts available such as sandwich, multi-spar vertical, multi-spar horizontal, multi-rib, net absorber, splitter, absorber elements concept. Schematically they are shown below.

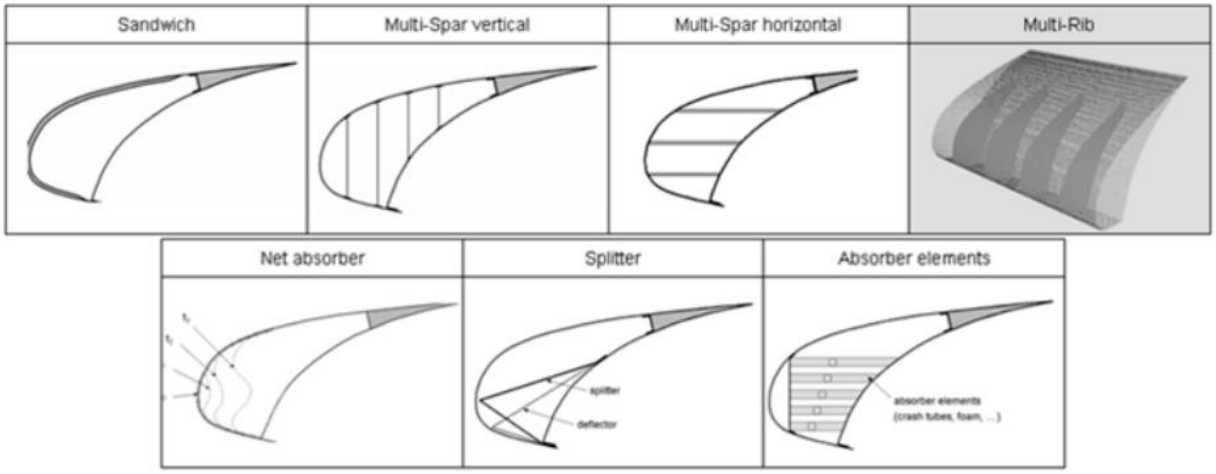

Figure 18 Various concepts for composite slat design

Because of showing best potential of energy absorption capacity **[7]**, the Multi-Rib concept was selected for further analysis.

3.2 Airplane prototype

Because of availability of technical and construction data **Boeing B737-200** was chosen as an airplane prototype. Wing geometry and FE models have been created based on information from technical manuals.

The Boeing 737-200 is a twin-engine short-range narrow body airliner with a capacity of maximum 136 passengers produced by the American manufacturer *Boeing Commercial Airplanes*.

3.3 Slat location

Designing slat is located on an outer part of the wing. Its location is shown below.

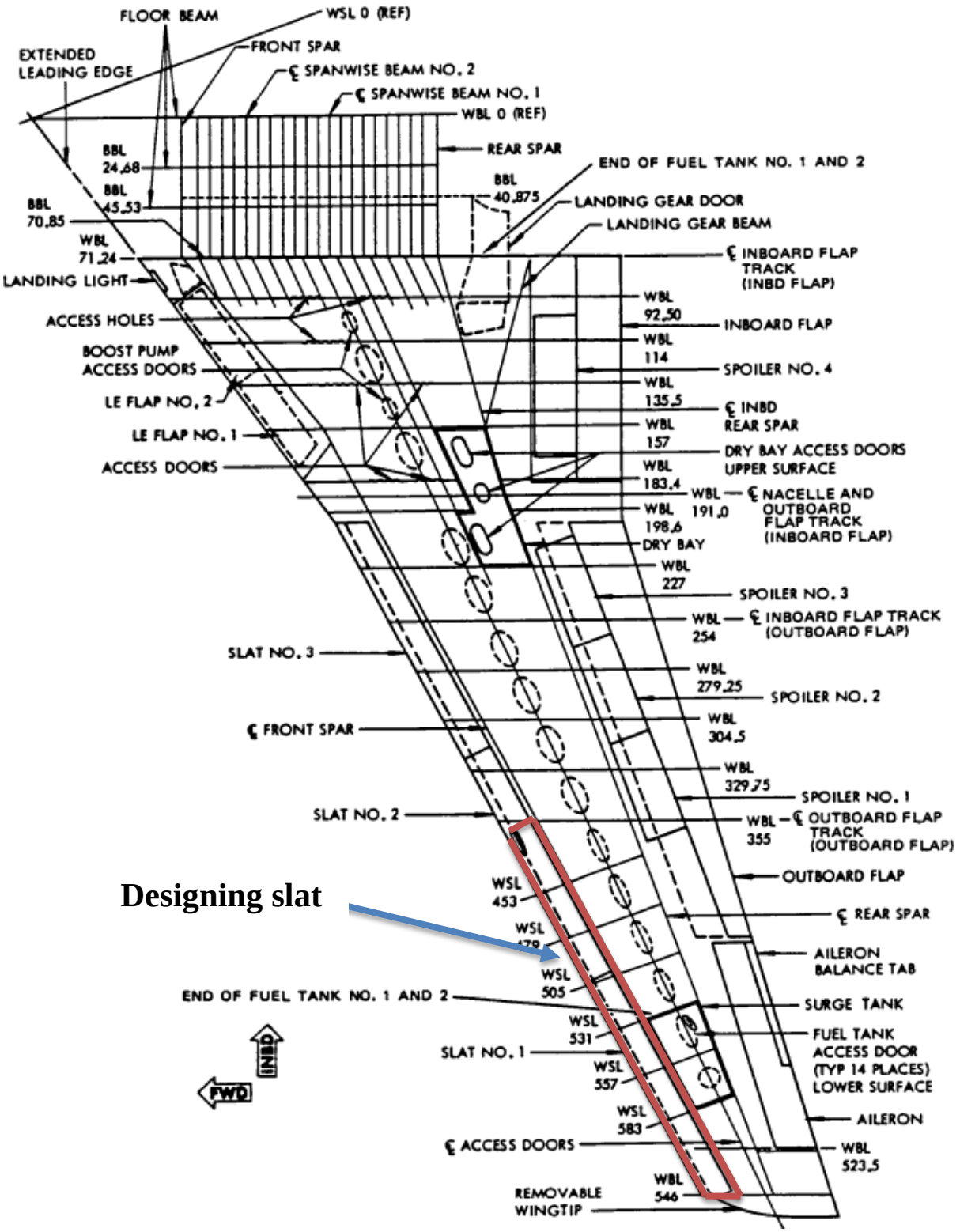

Figure 19 Slat location

3.4 Slat geometry

Original construction has three slats. In this project, these three slats will be substituted with two longer slats. Taking into account the fact that the end part of the wing has the least resistance to a bird strike (significantly smaller stiffness in compare to root section) the outer slat will be designed in this project.

3.4.1 CAD model

Airfoil geometry was taken from an earlier project [6]. CAD model was created in CATIA V5 software.

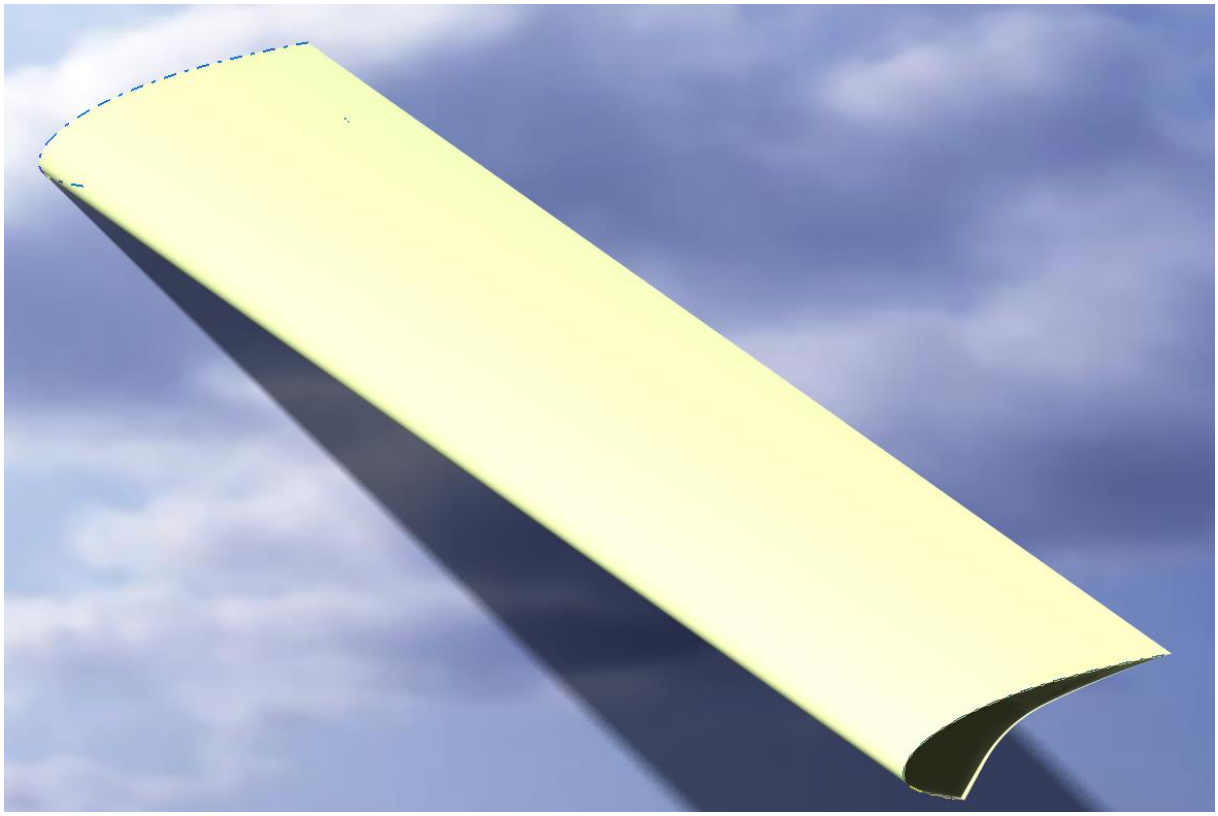

Figure 20 Slat CAD model

Geometric characteristics: length is 4773 mm, cross-section area is 4275,91 mm^2.

3.5 Slat attachment position

Attachment position was taken from [8] and shown below. In local coordinate system coordinates are: x = 30.75mm, y = -3.85mm

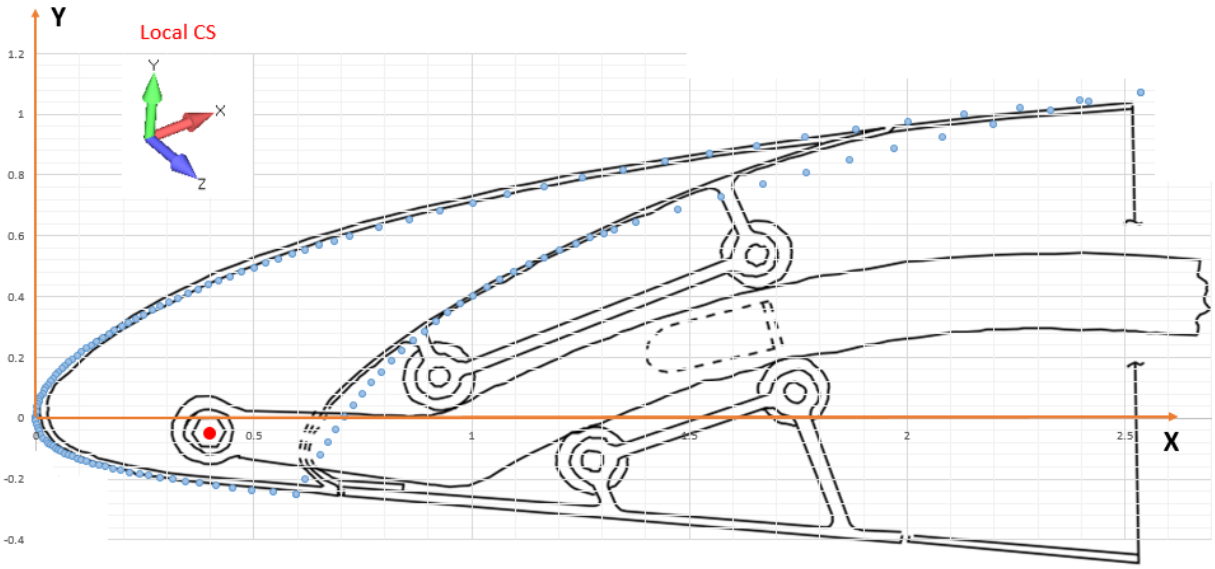

Figure 21 Attachment position in local CS

3.6 Material

IM7/8552 UD tape was chosen [9] for project purposes. The material properties are tabulated in Table 13 below.

Material props		
E1t	158830	MPa
E1c	143700	MPa
E2t	9100	MPa
E2c	9700	MPa
μ12	0.36	
μ21	0.02063	
G12s	4800	MPa
F1tu	2096	MPa
F1cu	1126	MPa
F2tu	81	MPa
F2cu	223	MPa
F12su	134	MPa
t0	0.125	mm

Table 13 IM7/8552 material properties

3.7 Slat loads

During the flight slat is loaded by aerodynamic forces, which are the main input for further calculations. Because of limited information accessible about the prototype only three load cases (take-off, cruise, landing) were chosen for further calculations. The maximum loads appeared to be in the take-off configuration [6], which parameters are shown below.

1.2 Take off configuration #5

m=62822kg (=MTOW)
M=0,34 (max speed with flaps #5)
H=0m
n=2 (flap envelope)
vIAS=115,6m/s (=416km/h=224,7KIAS)

Místo	Slot	Dutina	Flap 1	Flap 2	Flap 3	Celkem
ΔCL[-]	0,70	1,99	0,11	0,01	0,05	2,86
ΔCL[%]	24,48	69,58	3,85	0,35	1,75	100

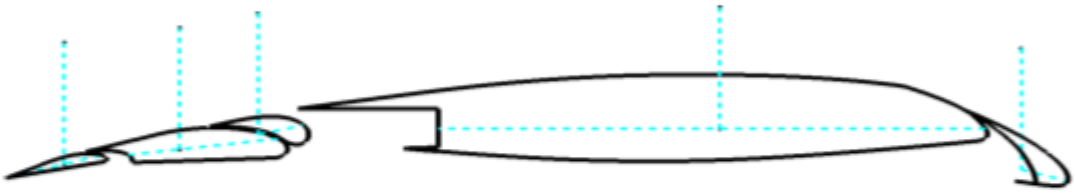

Místo	Slot	Dutina	Celkem
ΔCL[-]	0,70	2,16	2,86
ΔCL[%]	24,48	75,52	100

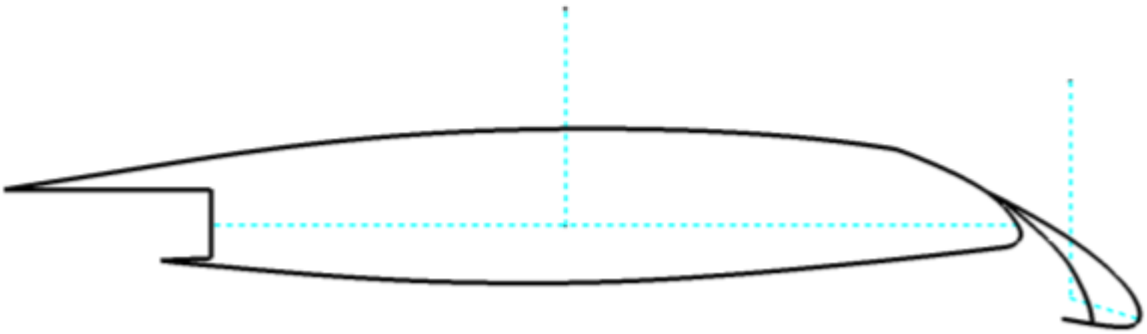

Figure 22 Take off configuration parameters

3.7.1 Analytical loadings calculation

Continuous load q taken from [6]. Safety factor is 1.725.

Limit loads[N/mm]	
q1	1.735
q2	5.839

Ultimate loads[N/mm]	
q1	2.993
q2	10.072

Table 14 Beam continuous loading

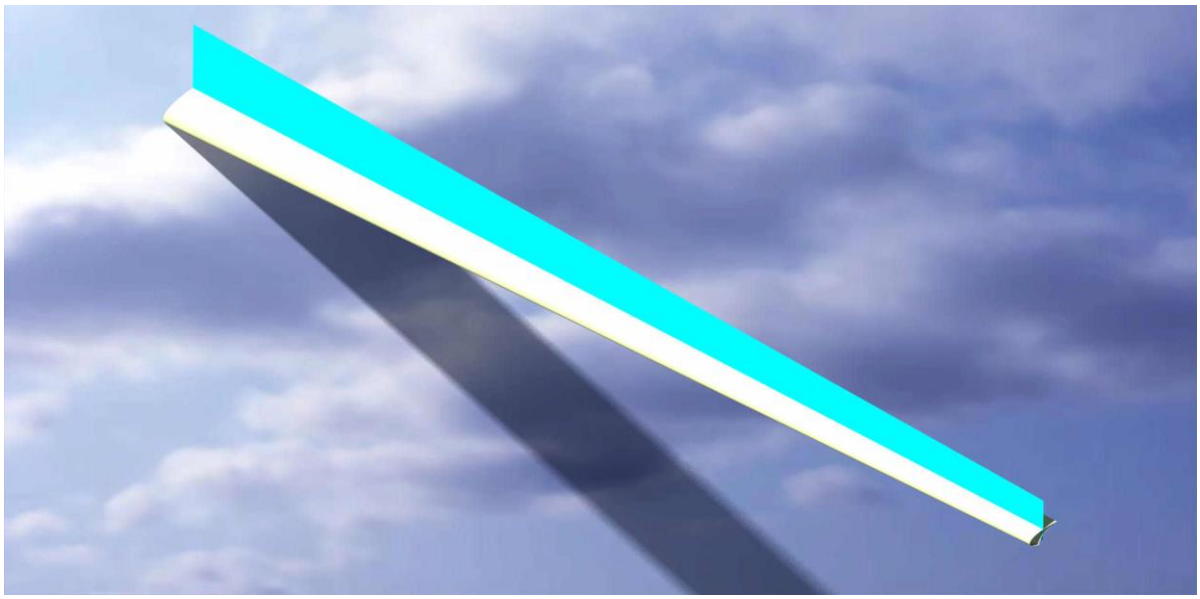

Figure 23 Wing continuous loading

During static analysis slat considered as a beam supported at three points. Internal load factors distribution along the slat was calculated in MINISTATIC software. The results are shown below.

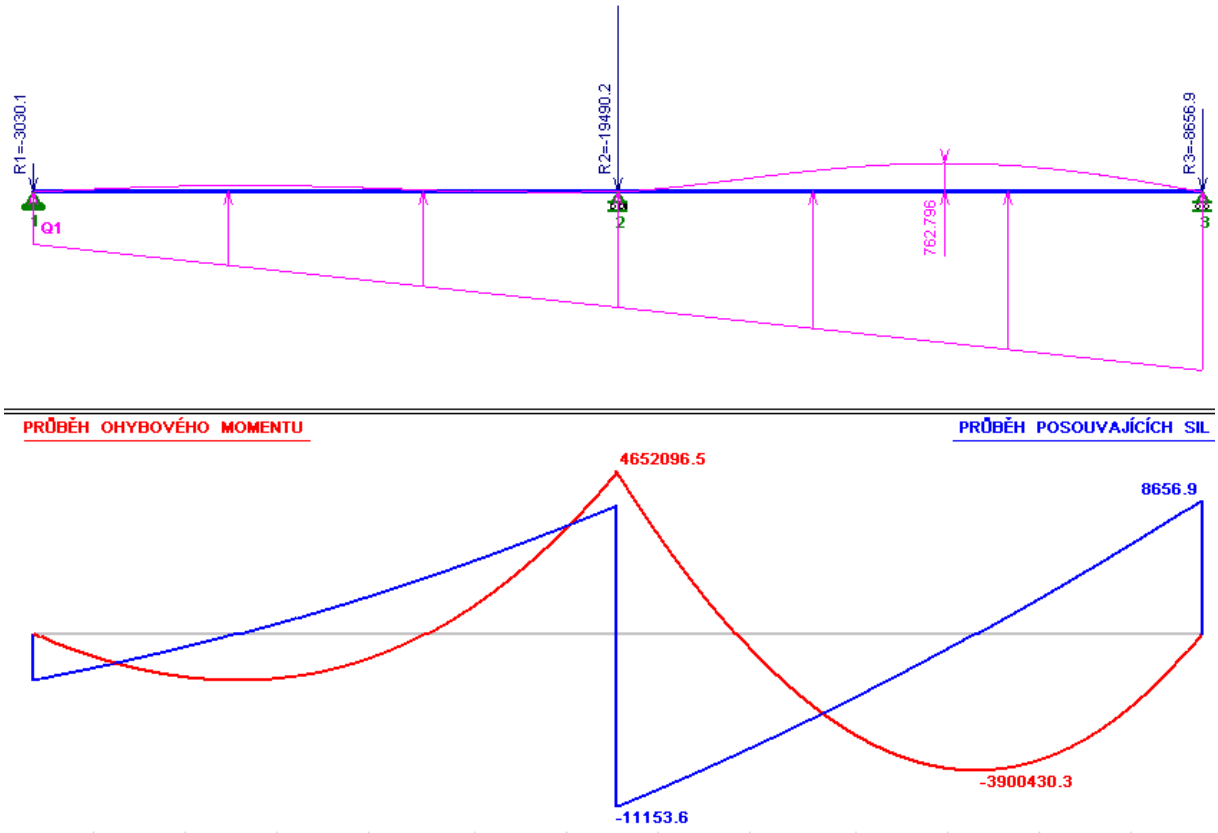

Figure 24 Beam static analysis

The maximum torsion moment (occurred close to the mid support) can be calculated from the next equation:

$$\boldsymbol{R \cdot a - T \cdot b = 0} \qquad \textbf{(1)}$$

where:

- R=19490 N – reaction at the middle support
- T=11154 N – the maximum shear force at the middle support
- a=60.93mm, b=3.4mm – forces arms

Note that the moment is calculated in relation to the elastic axis of the slat cross section. Schematically it is shown below on Figure 23.

Loading factor	Value
Shear force [N]	11154
Bending moment [N*mm]	4652097
Torsion moment [N*mm]	-1149780

Table 15 Beam loads

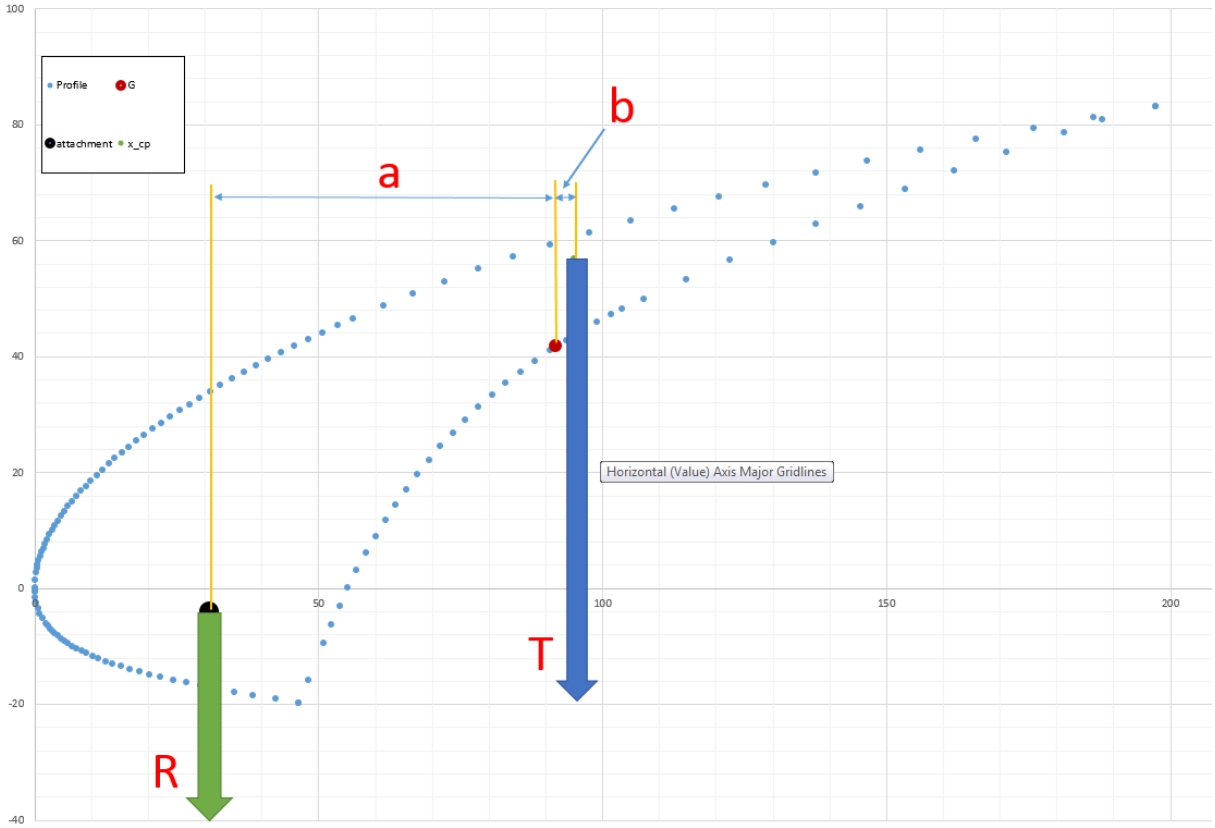

Figure 25 Slat torsion moment

3.8 Slat thickness calculation

The skin is planned to be made from a laminate with symmetrical balanced layup. According to the differential principle for composite thin-walled structure development the torsion moment and shear force are supposed to be taken by plies with ±45° orientation and bending moment by plies with 0° orientation. Because none forces act in transversal direction (-X in local CS) laminate has ±45°/0° layup.

3.8.1 Calculation methodology

Cross-sectional internal loads and stresses were calculated according to methodology [10]. The slat is considered as a thin-walled rod with a closed loop section with cross-section constant along the slat length.

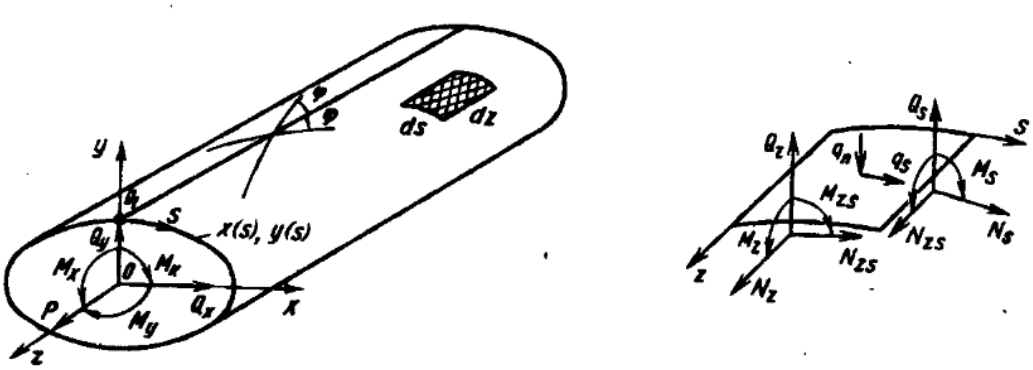

Figure 26 Composite rod geometrical parameters and loads

Torsion moment and shear force were calculated to the shear stresses flow **q** and bending moment to longitudinal forces **p**.

List of used equations is provided below.

Longitudinal forces:

$$p = B(s)\left[\frac{P}{S} + k\left(\frac{\overline{M_x}}{D_x^0}\overline{y} + \frac{\overline{M_y}}{D_y^0}\overline{x}\right)\right] \quad \textbf{(2)}$$

where $\overline{x} = x - x_0 - n_x(y - y_0), \overline{y} = y - y_0 - n_y(x - x_0),$

$$k = \frac{1}{1 - n_x n_y}, n_x = \frac{D_{xy}^0}{D_x^0}, n_y = \frac{D_{xy}^0}{D_y^0}, \overline{M_x} = M_x - y_0 P, \overline{M_y} = M_y - x_0 P \quad \textbf{(3)}$$

$$D_x^0 = D_x - y_0^2 S, D_x^0 = D_y - x_0^2 S, D_{xy}^0 = D_{xy} - x_0 y_0 S \quad \textbf{(4)}$$

$$x_0 = \frac{S_y}{S}, y_0 = \frac{S_x}{S}, S = \oint B\, ds,\ S_x = \oint B\, y ds,\ S_y = \oint B\, x ds,$$

$$D_x = \oint B\, y^2 ds,\ D_y = \oint B\, x^2 ds\ ,\ D_{xy} = \oint B\, xy ds \quad \textbf{(5)}$$

Where S is the elastic slat cross-section modulus,S_x, $S_y$are first moments of the slat cross-section area, D are inertia moments,

$B = E_x$- laminate Young's modulus in longitudinal direction

Because moment over y-axis $M_y = 0$ and axis force $P = 0$, equation (2) reduces to:

$$p = B(s) \cdot k \frac{\overline{M_x}}{D_x^0} \overline{y} \quad \textbf{(6)}$$

Shear flow:

$$q = q_0 + q_Q \quad \textbf{(7)}$$

where

$$q_Q = -k[\frac{Q_y}{D_x^0} \overline{S_x}(s) + \frac{Q_x}{D_y^0} \overline{S_y}(s)] \quad \textbf{(8)}$$

$$\overline{S_x}(s) = \int_0^s B\overline{y} ds, \overline{S_y}(s) = \int_0^s B\overline{x} ds \quad \textbf{(9)}$$

Where functions $\overline{S_x}(s), \overline{S_y}(s)$ are static moments of the cut part of the cross-section envelope at s-coordinate to x and y axis (see Figure 26), and Q_y, Q_x are shear forces

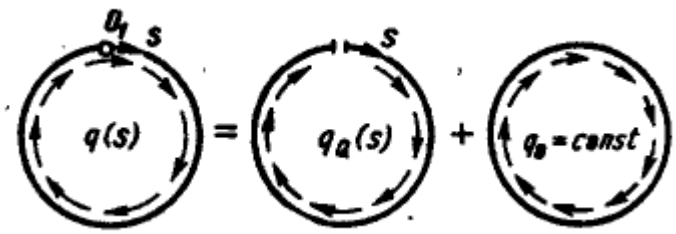

Figure 27 Shear stress flow

$$q_0 = \frac{1}{2F}(M_t + \oint q_Q \, r ds) \quad \textbf{(10)}$$

$$r = x \sin\beta + y \cos\beta \quad \textbf{(11)}$$

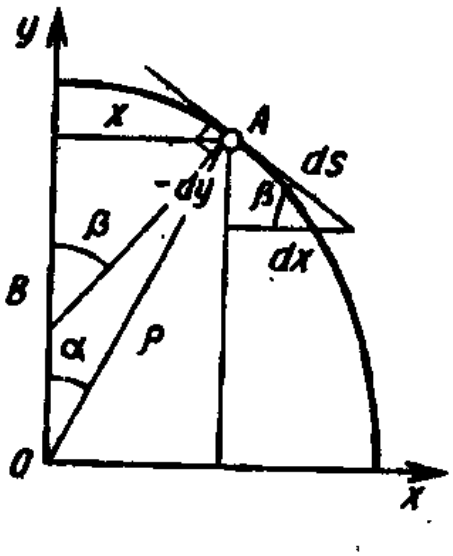

Figure 28 Composite rod geometrical parameters

Because $\boldsymbol{Q_x = 0}$, equation (6) reduces to:

$$q = -k\frac{Q_y}{D_x^0}\overline{S_x}(s) + \frac{1}{2F}(M_t + \oint q_Q\, r ds) \qquad \textbf{(12)}$$

Laminate properties were calculated according to methodology [11]

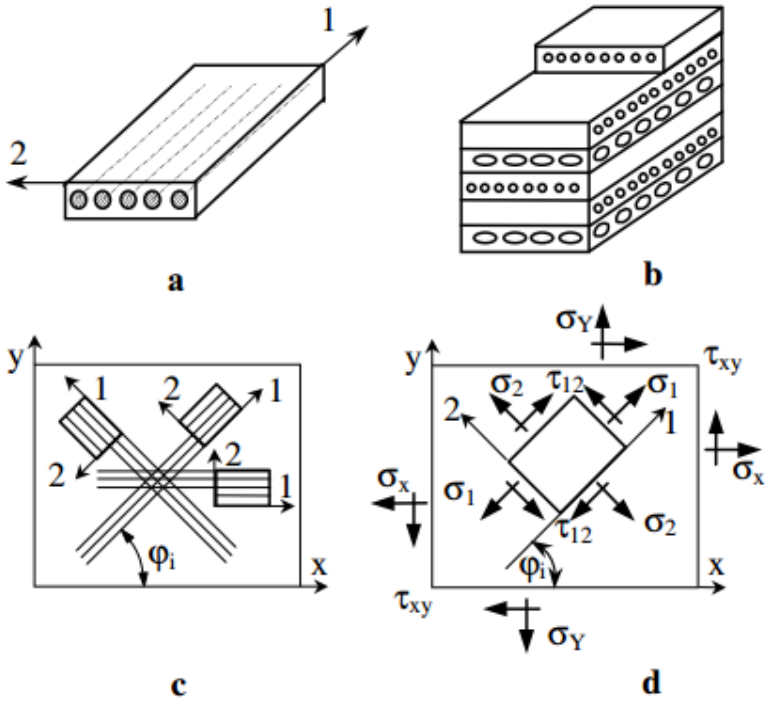

Figure 29 Formulation of composite properties (according to [11])

Formulas for determination of elastic properties of laminated composite materials follow from [11].

3.8.2 Calculation algorithm

Calculation done by the next iteration sequence:

1. Random number of ±45°/0° layers was set.
2. Stresses from shear stresses flow **q** and longitudinal forces **p** were calculated separately for plies in corresponding directions (±45° from **q**, 0° from **p**).
3. Reserve factor was calculated, and depend on its value the number of plies was corrected separately for corresponding reinforcement angle
4. Laminate properties (elastic constants) were determined
5. Laminate stresses σ_x, τ_{xy} were determined
6. Ply stresses were calculated for each ply angle (±45° and 0°)
7. Reserve factor was determined, and depend on its value the number of plies was corrected

Note, that target RF=1.10, critical stress is in compression.

3.8.3 Calculation results

Calculation in details can be found in supported document [12]. Resultant laminate properties, stresses, ply stresses and MSs are shown below.

p[N/mm]	q[N/mm]
-1616.88	-1851.45

Table 16 Internal cross-sections l load factors

Elastic constants											
E1i_[MPa]	E2i_[MPa]	n[-]	δ[mm]	ϕ[deg]	cosϕ	sinϕ	cos2ϕ	sin2ϕ			
160018.183	9168.08	15	0.125	45	0.707	0.707	0	1			
b11i	b12i=b21i	b22i	b13i=b31i	b23i=b32i	b33i	B11	B12	B22	B13	B23	B33
48746.8182	39146.82	48746.82	37712.53	37712.53	40646.31	91400.28	73400.284	91400.28	70710.99	70710.99	76211.83

Table 17 Plies elastic constants, 45° plies

Elastic constants											
E1i_[MPa]	E2i_[MPa]	n[-]	δ[mm]	ϕ[deg]	cosϕ	sinϕ	cos2ϕ	sin2ϕ			
160018.183	9168.08	15	0.125	-45	0.707	-0.707	0	-1			
b11i	b12i=b21i	b22i	b13i=b31i	b23i=b32i	b33i	B11	B12	B22	B13	B23	B33
48746.8182	39146.82	48746.82	-37712.53	-37712.53	40646.31	91400.28	73400.284	91400.28	-70711	-70711	76211.83

Table 18 Plies elastic constants, -45° plies

Elastic constants											
E1i_[MPa]	E2i_[MPa]	n[-]	δ[mm]	ϕ[deg]	cosϕ	sinϕ	cos2ϕ	sin2ϕ			
160018.183	9168.08	10	0.125	0	1	0	1	0			
b11i	b12i=b21i	b22i	b13i=b31i	b23i=b32i	b33i	B11	B12	B22	B13	B23	B33
160018.183	3300.51	9168.076	0	0	4800	200022.7	4125.6341	11460.09	0	0	6000

Table 19 Plies elastic constants, 0° plies

Laminate elastic constants								
Ex[MPa]	Ey[MPa]	μ_xy	μ_yx	Gxy[MPa]	ηxy,x	ηxy,y	ηx,xy	ηy,xy
53112.95	26951.75	0.777	0.394	31684.7332	0	0	0	0

Membrane stiffeness							
B[N/mm]	B11[N/mm]	B12[N/mm]	B22[N/mm]	B13[N/mm]	B23[N/mm]	B33[N/mm]	δΣ[mm]
8.17E+15	382823.30	150926.20	194260.66	0	0	158423.666	5

Table 20 Laminate properties

Laminate loads		
σx[MPa]	σy[MPa]	τxy[MPa]
-323.38	0	-370.29

Table 21 Laminate stresses

Ply effective stress									
a11i	a12i	a13i	a21i	a22i	a23i	a31i	a32i	a33i	ϕ[deg]
2.1E-06	1.12E-05	1.58E-05	2.10E-06	1.12E-05	-1.58E-05	0	0	0	45
σ_1i[MPa]	σ_2i[MPa]	τ_12i[MPa]							
-1026.66	25.82	52							

Table 22 Ply stress in local CS 12, 45° plies

Ply effective stress									
a11i	a12i	a13i	a21i	a22i	a23i	a31i	a32i	a33i	ϕ[deg]
2.1E-06	1.12E-05	-1.58E-05	2.10E-06	1.12E-05	1.58E-05	0	0	0	-45
σ_1i[MPa]	σ_2i[MPa]	τ_12i[MPa]							
804.85	-42.75	-52							

Table 23 -45°

Ply effective stress									
a11i	a12i	a13i	a21i	a22i	a23i	a31i	a32i	a33i	ϕ[deg]
1.883E-05	-1.46E-05	0	-1.46E-05	3.71E-05	0	0	0	0	0
σ_1i[MPa]	σ_2i[MPa]	τ_12i[MPa]							
-958.65	23.27	-56							

Table 24 0°

ply orientation[deg]	RF_1	RF_2	RF_3
0°	1.10	3.14	2.57
45°	2.60	5.22	2.57
-45°	1.17	3.48	2.38

Table 25 Ply reserve factors

Resultant laminate stacking sequence is $[\pm 45_2/(\pm 45/0)_5]_s$, overall thickness t=5mm.

3.9 FE stress analysis of the slat

3.9.1 FE model description

Slat FE model was created for stress analysis. Model was created in ANSA software by shell elements. Model geometry was taken from Catia CAD model. MAT8 material model was chosen for the composite ply. Laminate was defined by PCOMP property type. Boundary conditions were defined by SPC1 elements, connections by RBE2 elements. Aerodynamic loads were applied at the cross-sectional centers of pressure as resultant nodal forces Inertia forces were applied as an acceleration.

Model attachments are defined in 3 points:

- Point 1 - 1,2,3,6 DOF's were taken in local CS system
- Point 2 - 1,2,6 DOF's were taken
- Point 3 - 1,2,6 DOF's were taken

Loads were taken from [6]

3.9.2 Slat FE simulation

3.9.2.1 Static stress analysis

Stress analysis of the structure developed in chapter 3.7 was done in NX NASTRAN v.9.0. Solver type – SOL101, Linear Static.

Post processing was done in FEMAP software. The analysis has shown that the skin thickness was overestimated by the analytical calculations and could be reduced. Number of ±45° layers was decreased to6, 0° layers to 8. Resultant laminate stacking sequence is $[(\pm 45/0)_3/0]_s$, overall thickness t is 2.5mm. The FE analysis of the structure with the new stacking sequence showed that max. stresses occur in ply No. 2. Results are shown in Tables 26, 27 and figures 30 - 32below.

orientation	σ_t[MPa]	σ_c[MPa]	τ[MPa]
L	1145	1017	57.51
T	48.48	27.17	

Table 26 Ply 2 stresses

orientation	RF_1	RF_2	RF_3
L	1.83	1.11	2.32
T	1.67	8.21	

Table 27 Ply 2 reserve factors

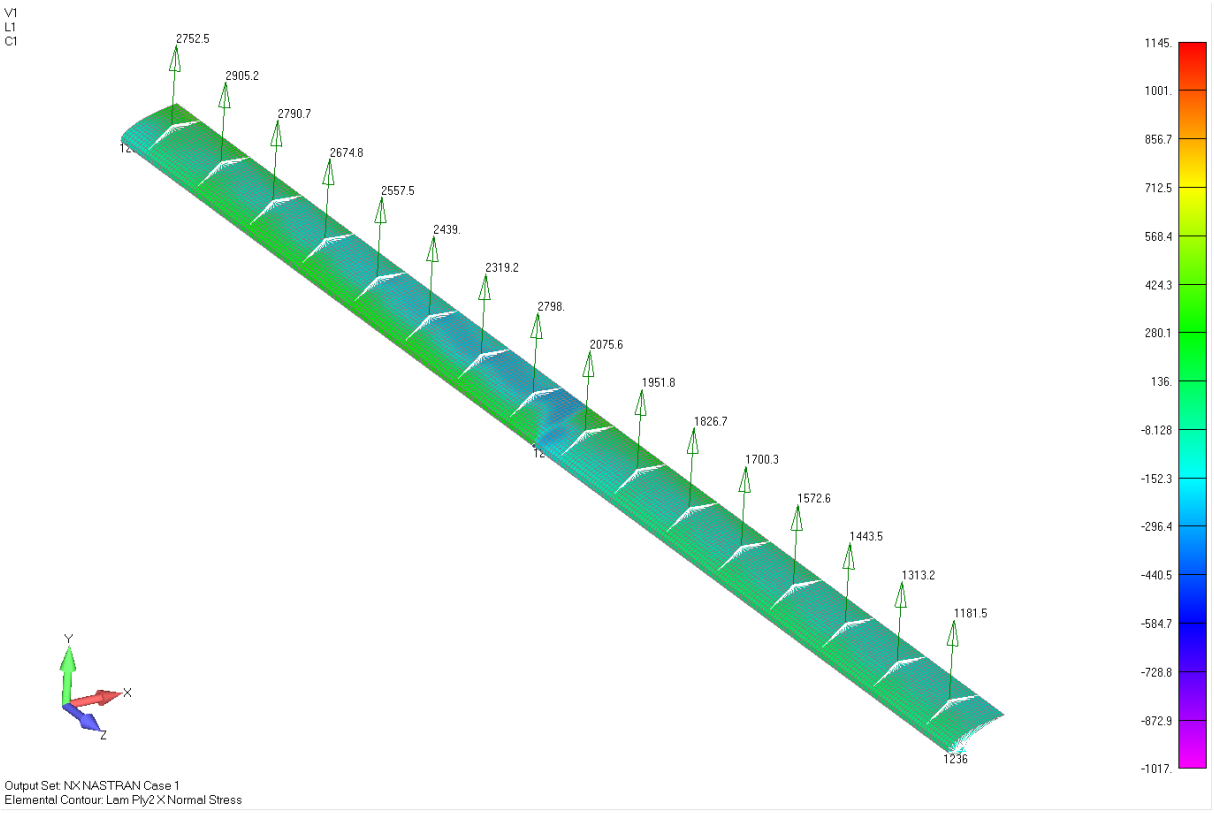

Figure 30 Ply 2 stresses, longitudinal

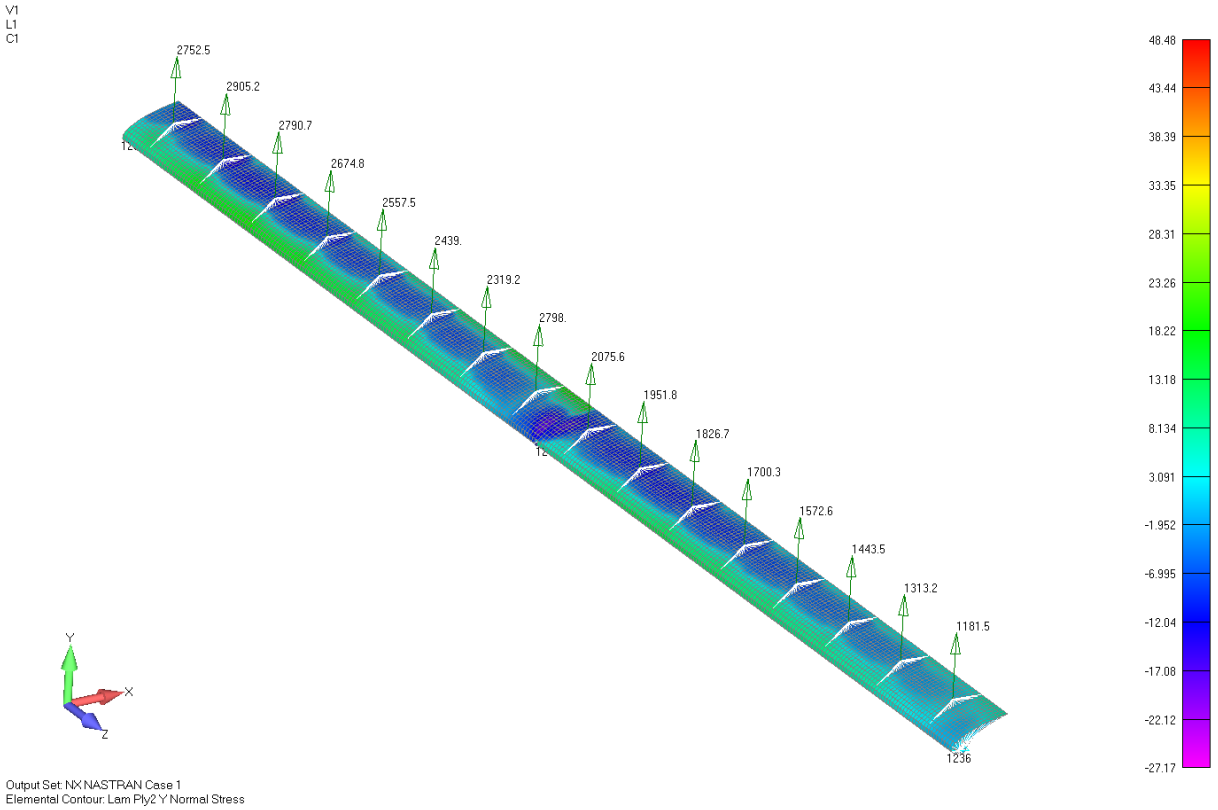

Figure 31 Ply 2 stresses, transversal

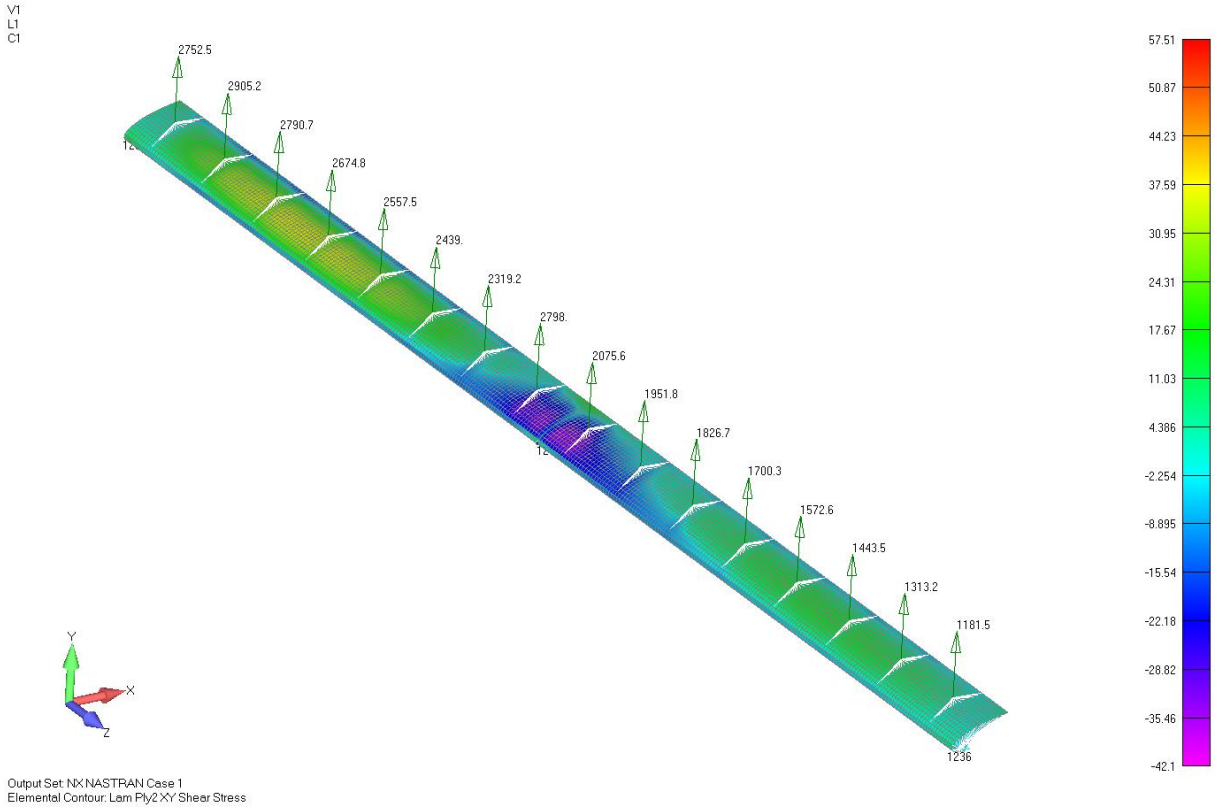

Figure 32 Ply 2 shear stresses

3.9.2.2 Buckling analysis

Buckling analysis was performed in NX NASTRAN v.9.0 also. Solver type – SOL105, Linear Buckling Analysis.

The analysis has shown that the structure loses stability at 86% of applied loads (Eigen number λ is 0.86).Therefore, two 0° plies have been added to the skin. As a result, minimum Eigen number λ grew up to 1.201 (see Figure 33). That means the structure will be stable at applied loads.

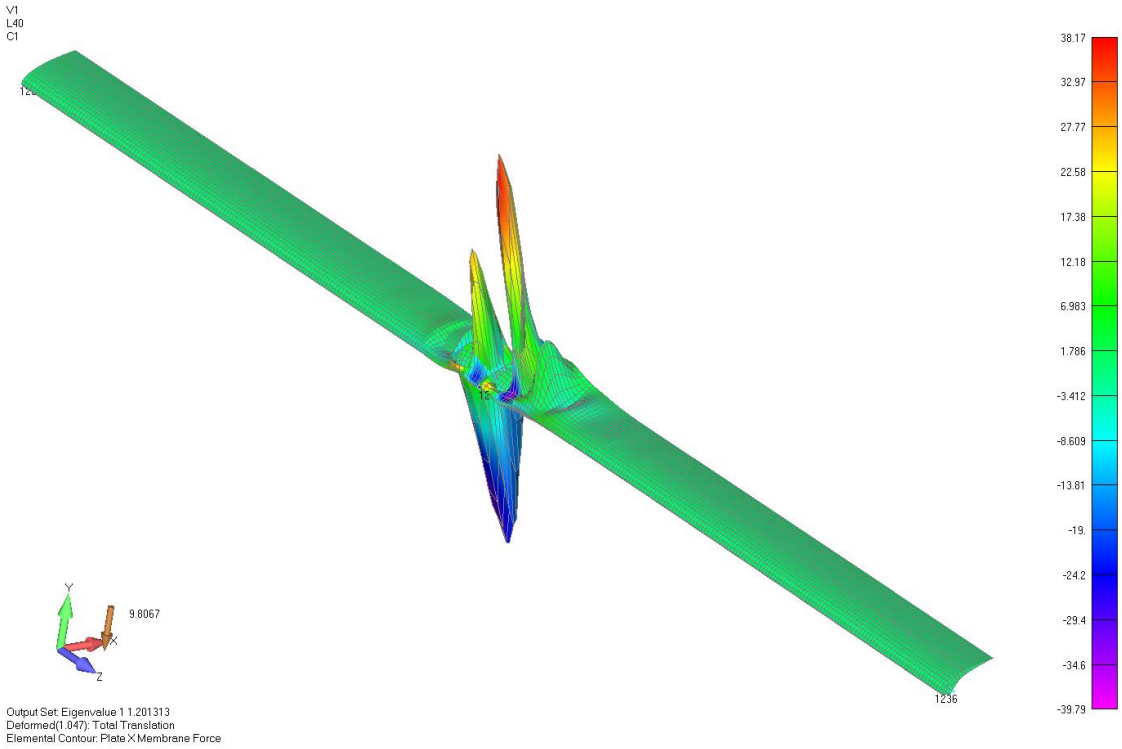

Figure 33 Slat X Membrane force, Eigenvalue λ = 1.201

3.10 Wing deflection influence

In order to assess slat behavior with respect to a wing deflection during corresponding phase of the flight, slat attachments translations have been measured. It was done by loading of the wing with aerodynamic forces for three load cases (take-off, cruise, landing). Attachments were connected to the wing by MPC2 and CROD elements. Based on these translations the slat was loaded again by aerodynamic forces. Slat deflections were measured according to the wing deflection. Maximum wing deflection and corresponding slat deflections are showed on Figure 34, 35 below.

	Translation		
att. ID[-]	x[mm]	y[mm]	z[mm]
131676	104	437	13
131677	62.6	267	12
131680	28.2	123	10

Table 28 Attachments translations, take-off load case

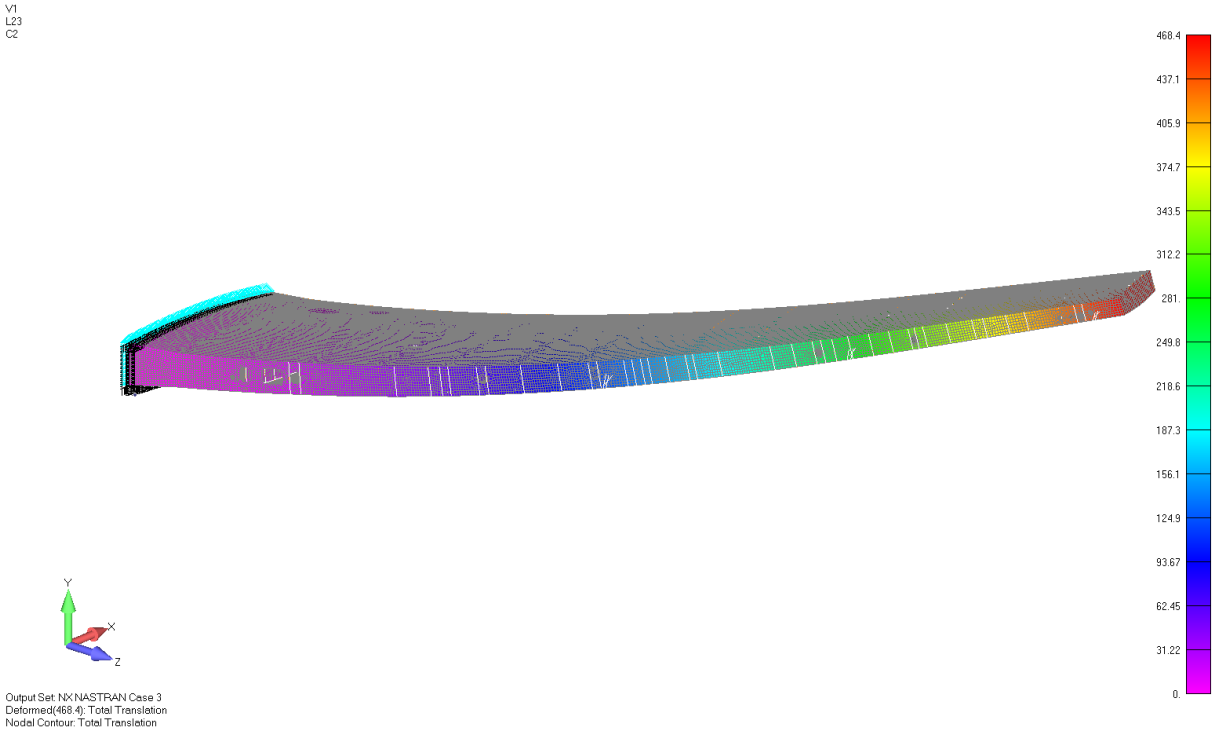

Figure 34 Wing deflection, take-off load case

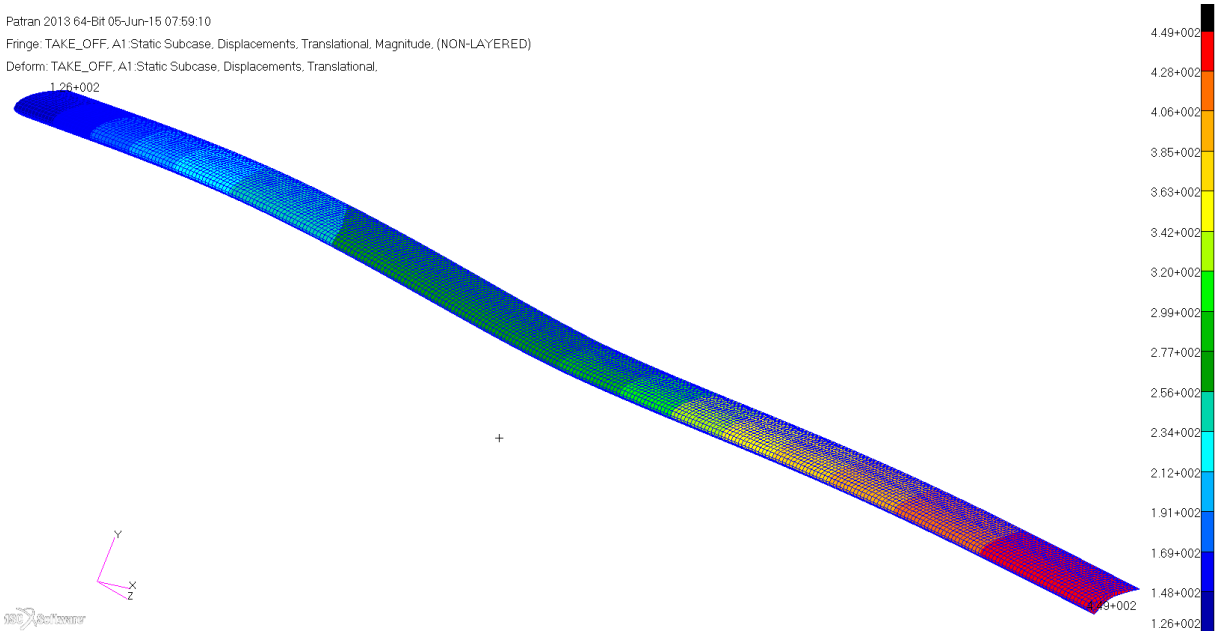

Figure 35 Slat deflections, take-off load case

3.11 Slat construction recalculation

Simulation made in chapter 3.10 showed that maximum slat deflection (50.9mm) is too high. In order to decrease its value it is needed to increase construction stiffness. As a way to do that increasing number of attachments was chosen. All previous analysis made in chapter 3.9 were done again. Slat frame and rib thickness decreased to 1.5mm.

Maximum stresses occur in Ply 1. Stresses and reserve factors are tabulated below.

orientation	σ_t[MPa]	σ_c[MPa]	τ[MPa]
L	1147	1003	51.94
T	62.55	49.38	

Table 29Ply 1 stresses

orientation	RF_1	RF_2	RF_3
L	1.83	1.12	2.6
T	1.29	4.52	

Table 30Ply 1 reserve factors

Maximum slat deflection is 11 mm.

3.12 Slat construction summary

After completing analytical calculation and numerical simulation, it was decided:

- Slat frame thickness is 1.5 mm
- Result frame laminate structure is $[(\pm 45/0)_2]_s$
- Slat ribs thickness is 1.5 mm
- Result rib laminate structure is $[\pm 45]_{3s}$.

FEM model has been upgraded according to revised parameters.

4 Bird strike simulation

Bird strike incidents cause significant flight safety threats to flying aircraft. Only in the States of America, each year, 36,000 aircraft accidents, produced by bird-strike, are estimated, and since 1988, wildlife strikes have killed more than 194 people and destroyed over 163 aircrafts. In the US, 92% of the strikes occur at below 3000 feet (920m) and 97% of the reported strikes occur during the taking off and landing phase of the aircraft [13]. Population development of large flocking birds has increased dramatically in many parts of the world. Nowadays bird-strike becomes a design requirement. Bird strike analysis involves nonlinear dynamics (material and geometric), contact/coupling, failure mods, large displacements, and other complexities [14]. During bird-strike investigations, it is needed to focus on:

- Residual strength and stiffness of damage structure.
- Aerodynamic loading on damaged structure.
- Ability of an airplane to continue flight and land safely("Get Home")

4.1 Bird modelling

Bird is non-homogenous, which is the main limitation in order to obtain repeatable results of tests. According to hydrodynamic theory [15], material strength and the response of the target material to the impact pressures can be neglected, the bird will be considered homogenous to simplify the problem. Schematically the bird impact is shown below.

Wilbeck and Rand [13] conducted that a mixture of 85-90 volume percent water and 10-15% of air can accurately model a real bird analytically, with a slightly increased density for water of 1.06*g/cm* 3. For this purpose, they recommended that a gelatin bird with 15% porosity (to account for the ads in real birds) represent a real bird accurately.

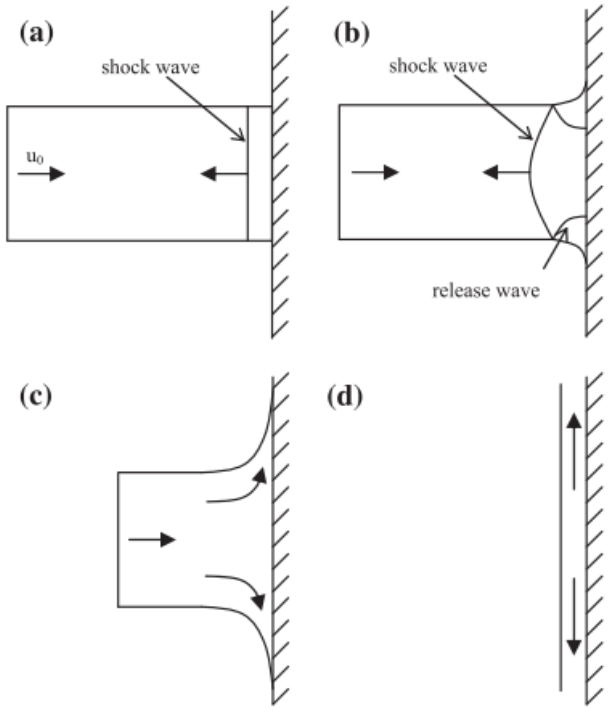

Figure 36 The phases of bird influence (a) initial impact, (b) shock decay, (c) steady flow, and (d) pressure decay (according to [15])

4.2 Bird modelling methods

In recent years, explicit FE codes have been used to develop high efficiency bird-proof structures. These codes adopted various finite element approaches to model the impact phenomena: the Lagrangian approach, Eulerian or Arbitrary Lagrangian Eulerian (ALE) approach, and recent solvers based on Smoothed Particle Hydrodynamics (SPH) [16].

4.2.1 Lagrangian modelling

The Lagrangian modeling method is the standard approach for most structural finite element analyses. The nodes of the Lagrangian mesh are associated to the material and therefore each node of the mesh follows the material under motion and deformation. This approach is typically used for solid materials. The major problem of Lagrangian bird impactor models are the severe mesh deformations. Large distortions of the elements may lead to inaccurate results, severe hour glassing and even error termination due to negative volume elements. Nowadays this method is considered as an impractical way in bird-strike modelling [16].

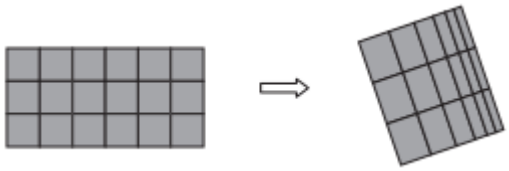

Figure 37 Lagrangian model: nodes are fixed to the material

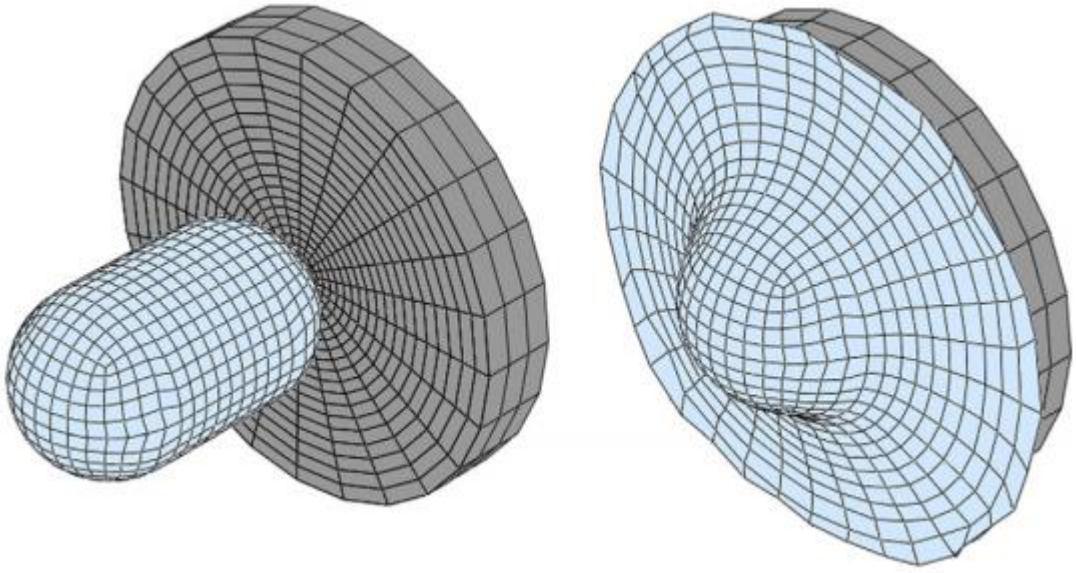

Figure 38 Bird strike simulation on rigid plate with Lagrangian impactor model

4.2.2 Eulerian modelling

In the alternative Eulerian method, the mesh remains fixed in space and the material flows through the mesh. Because the mesh does not move, mesh deformations do not occur and the explicit time step is not influenced. Stability problems due to excessive element deformation do not occur. This approach is typically used for fluid materials and flow processes. Each element has a certain volume fraction of different materials, those can be for example a fluid material and void, or even other materials. This means that each element may be partially filled

with the fluid material. The problem of this solver is numerical leakage, due to dissipation and dispersion problems associated with flux of mass between elements. The computational domain for structural analysis with the Eulerian technique is much larger than with the Lagrangian approach, which leads to high cost of this model, due to the high number of elements and the cost-intensive calculation of element volume fractions [16]. The element size of the Eulerian mesh has to be defined very small in order to achieve accurate results.

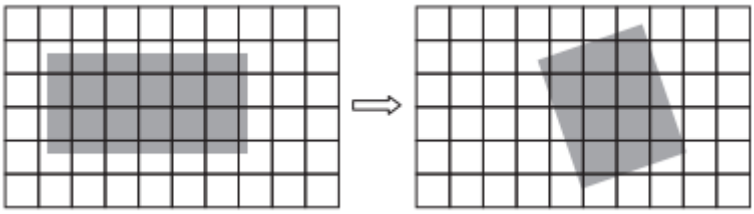

Figure 39 Eulerian model: nodes stay fixed and material flows through the mesh

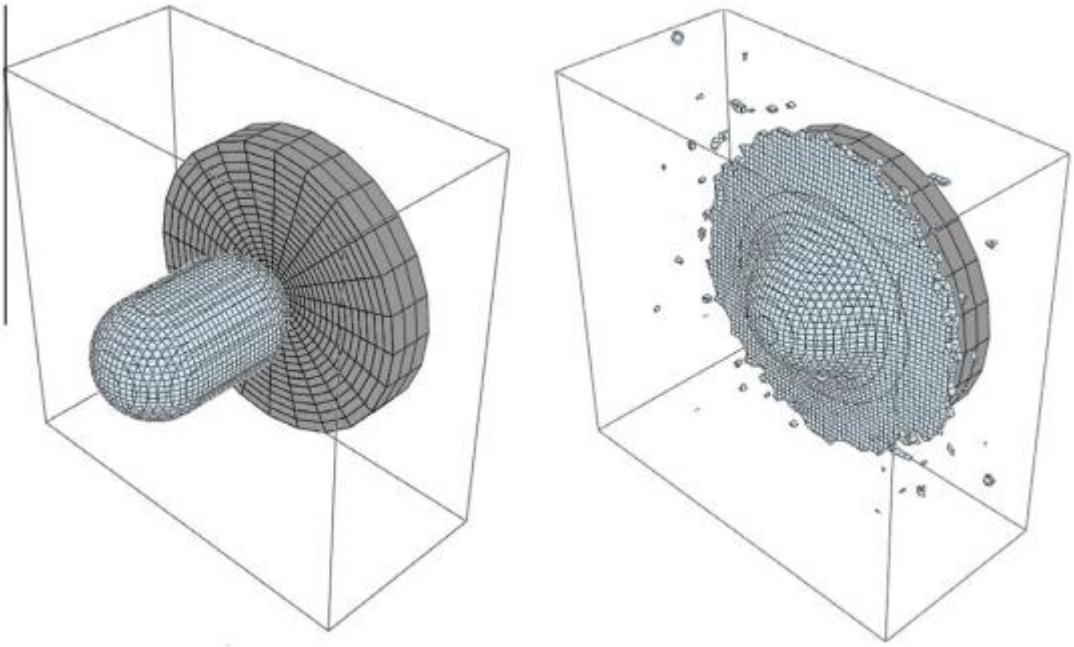

Figure 40 Bird strike simulation on rigid plate with Eulerian impactor model

4.2.3 Arbitrary Lagrangian Eulerian (ALE) modelling

Since in a bird strike simulation typically only the impactor is modeled as a fluid-like body with Eulerian elements and the target as a solid structure with Lagrangian elements, a coupled Eulerian-Lagrangian approach is used for this fluid structure interaction problem. Because the mesh in the classical Eulerian technique is fixed in space, the computational domain should cover not only the region where the material currently exists, but also additional void space to represent the region where material may exist at a later time of interest [16]. In the ALE method the surrounding Eulerian box can move and stretch if needed and is not fixed in space. Results accuracy depends on mesh quality.

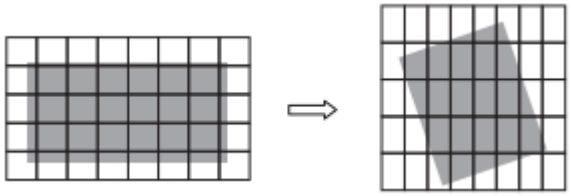

Figure 41 ALE model: Eulerian mesh moves and deforms with material flowing inside

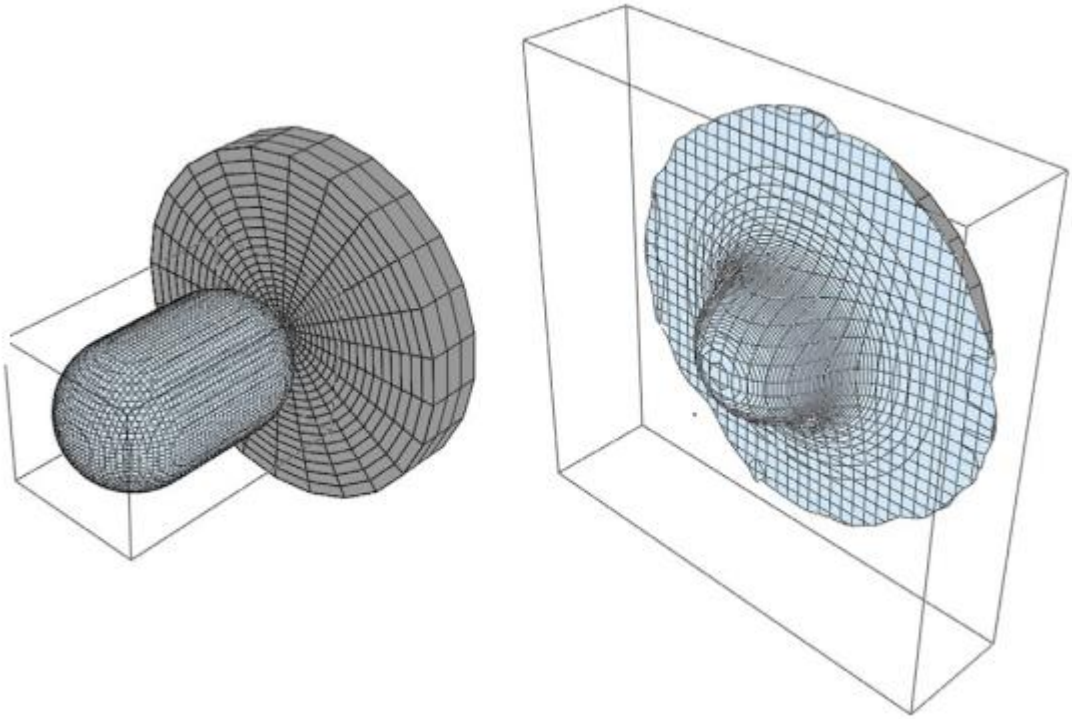

Figure 42 Bird strike simulation on rigid plate with ALE impactor model

4.2.4 Smoothed Particle Hydrodynamics (SPH) modelling

The SPH method is a meshless Lagrangian technique, based on interpolation theory and smoothing kernel functions. The fluid is represented as a set of discrete interacting particles (Figure 44), which are independent from each other. Each particle has a mass, velocity and material law assigned to it, which is not localized but smoothed in space by a smoothing kernel function, typically based on a B-spline approximation, defining the range of influence of the particle. Compared to the conventional solid Lagrangian mesh the time step is constant. However, in order to achieve accurate results particle density is required, which needs high memory resources. In comparison to Eulerian modelling the SPH method requires fewer elements, avoids the material interface problems associated with it and normally has a shorter solution time. Disadvantages of the SPH are the lack of sharp boundaries (it is difficult to apply boundary conditions), tension instability (numerical collapse and unphysical clustering of the particles under tension due to negative pressures), undefined impact area (SPH particles do not have a foot print) [16].

Figure 43 SPH model: fluid is modelled by particles with free motion

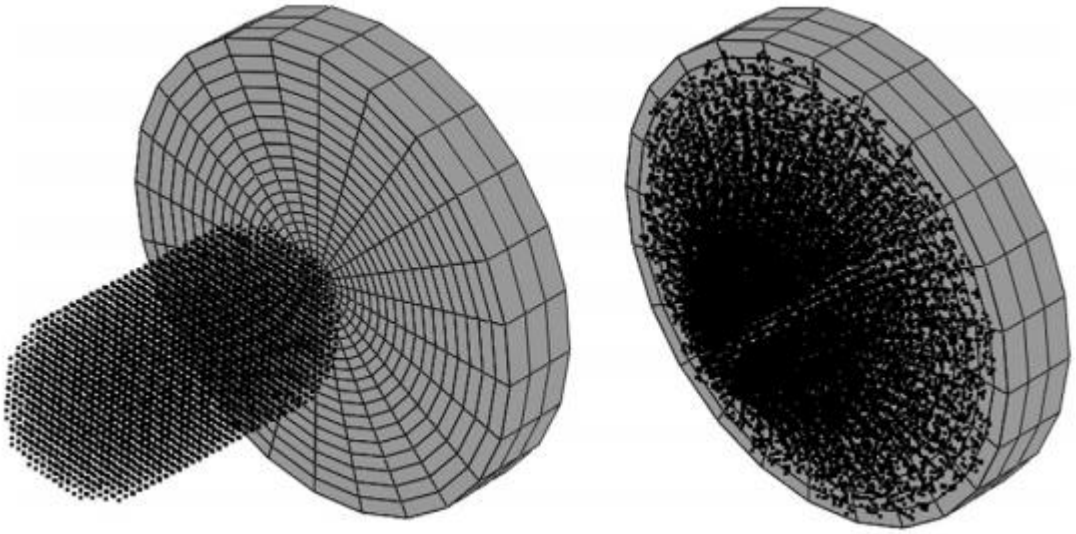

Figure 44 SPH model

4.3 Bird-strike simulation in MSC.Dytran software

4.3.1 Simulation conditions

The bird strike simulation was performed using ALE technique. The FE model was created with help of [17], [18].The slat model was taken from section 3.12.

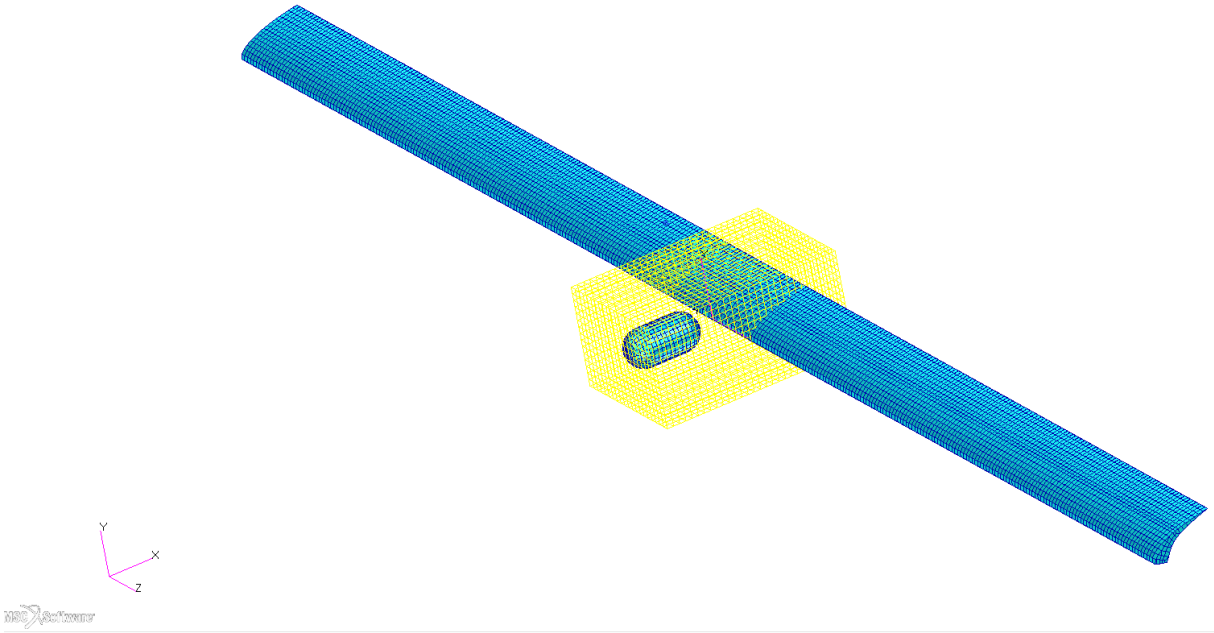

Figure 45 Bird strike simulation in Dytran

4.3.2 Simulation results

Slat stresses are shown below

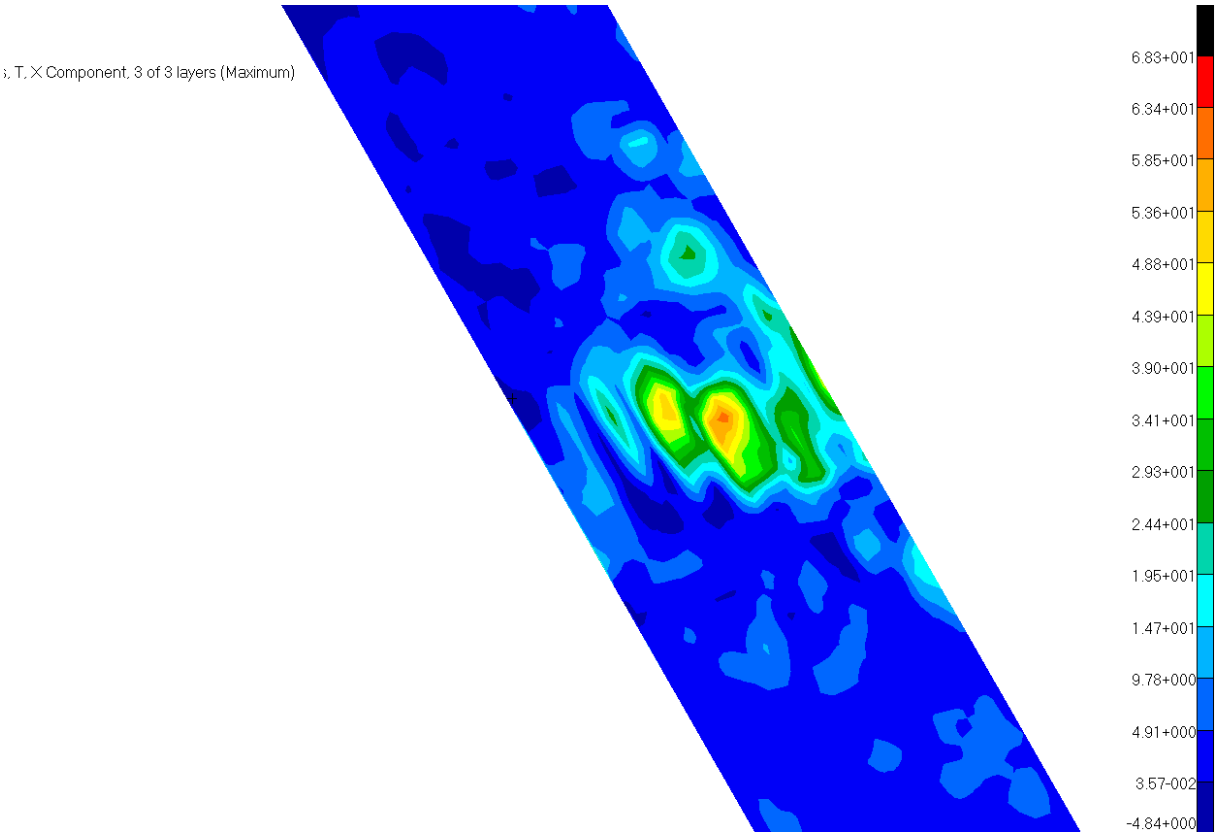

Figure 46 Slat stresses in tension, longitudinal

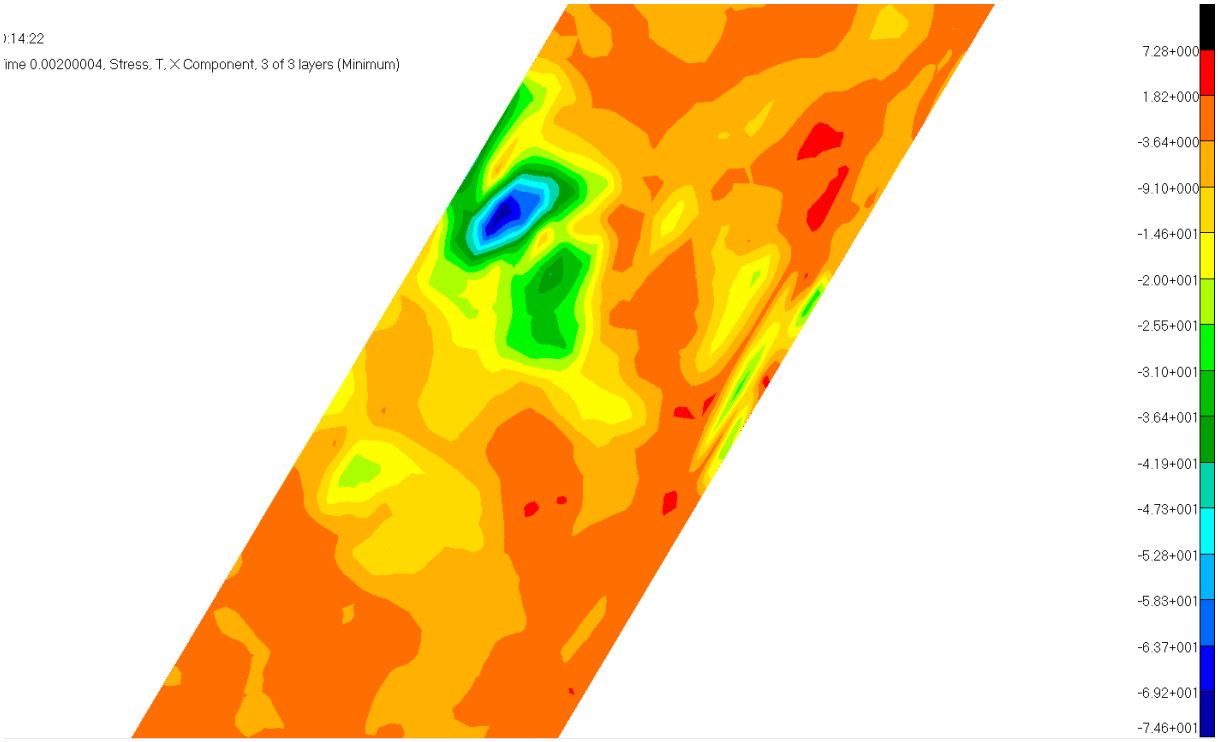

Figure 47 Slat stresses in compression, longitudinal

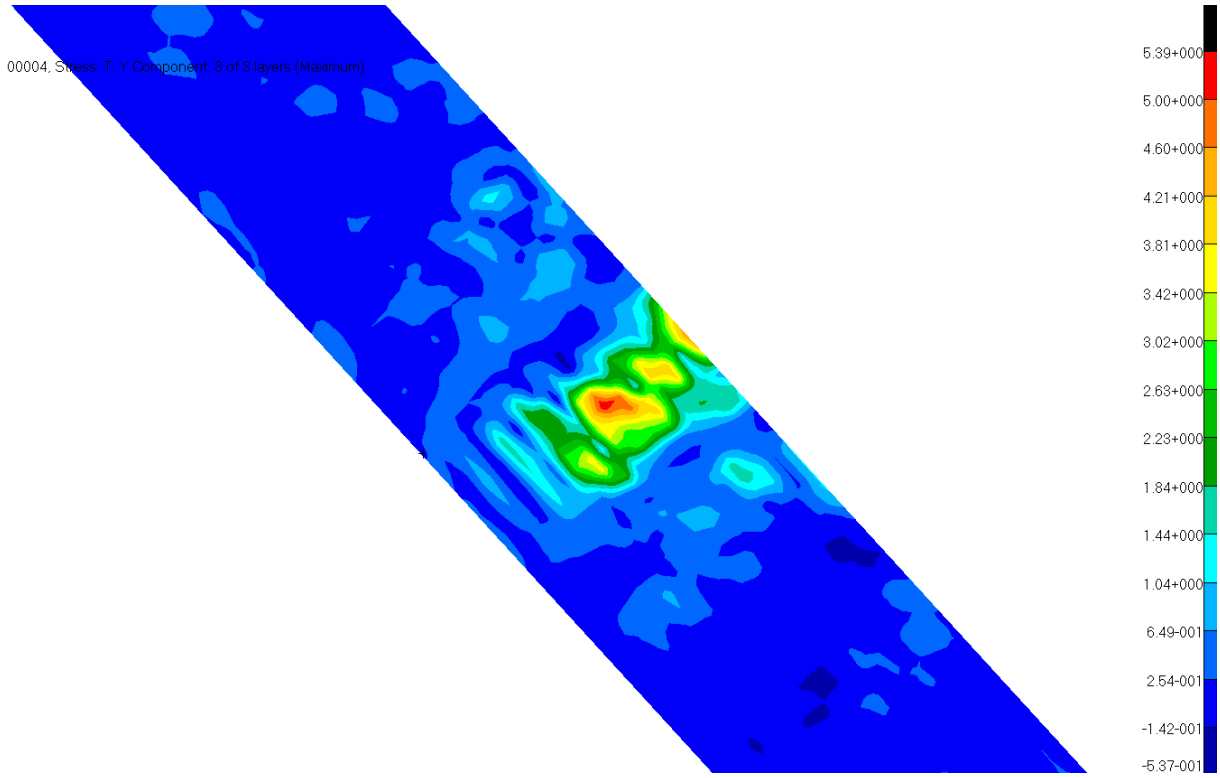

Figure 48 Slat stresses in tension, transversal

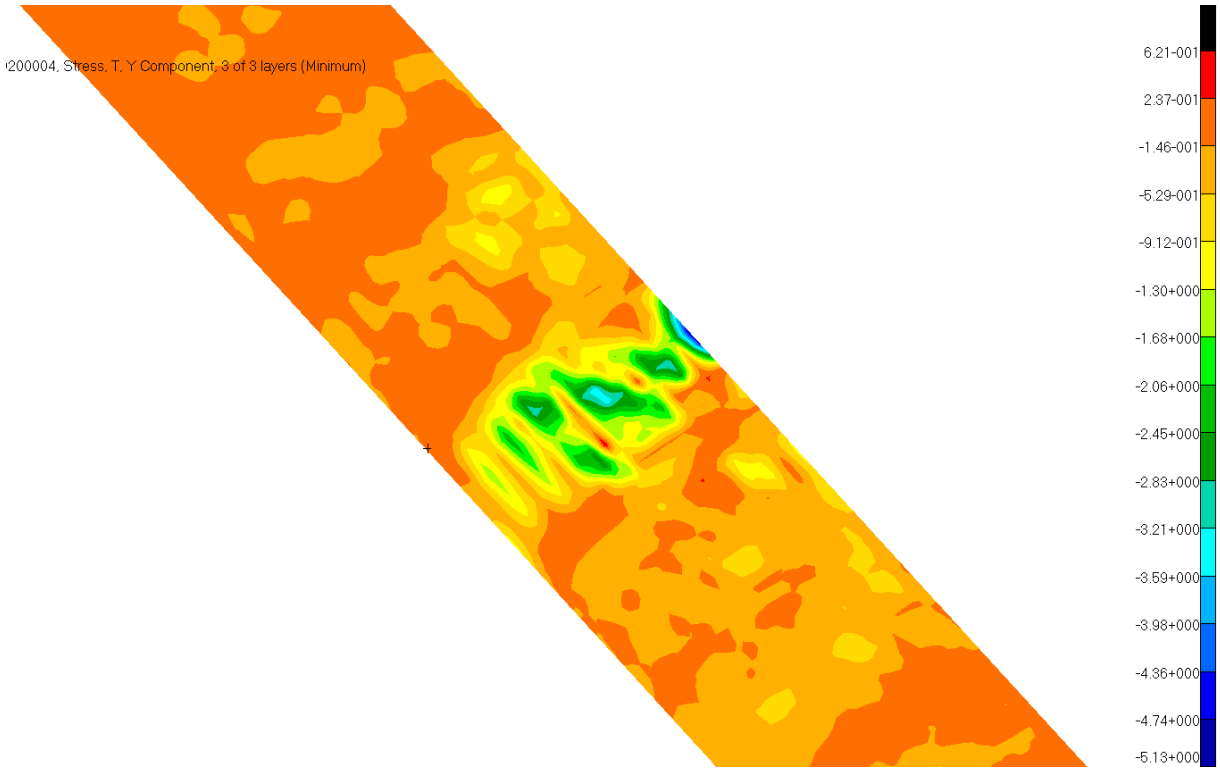

Figure 49 Slat stresses in compression, transversal

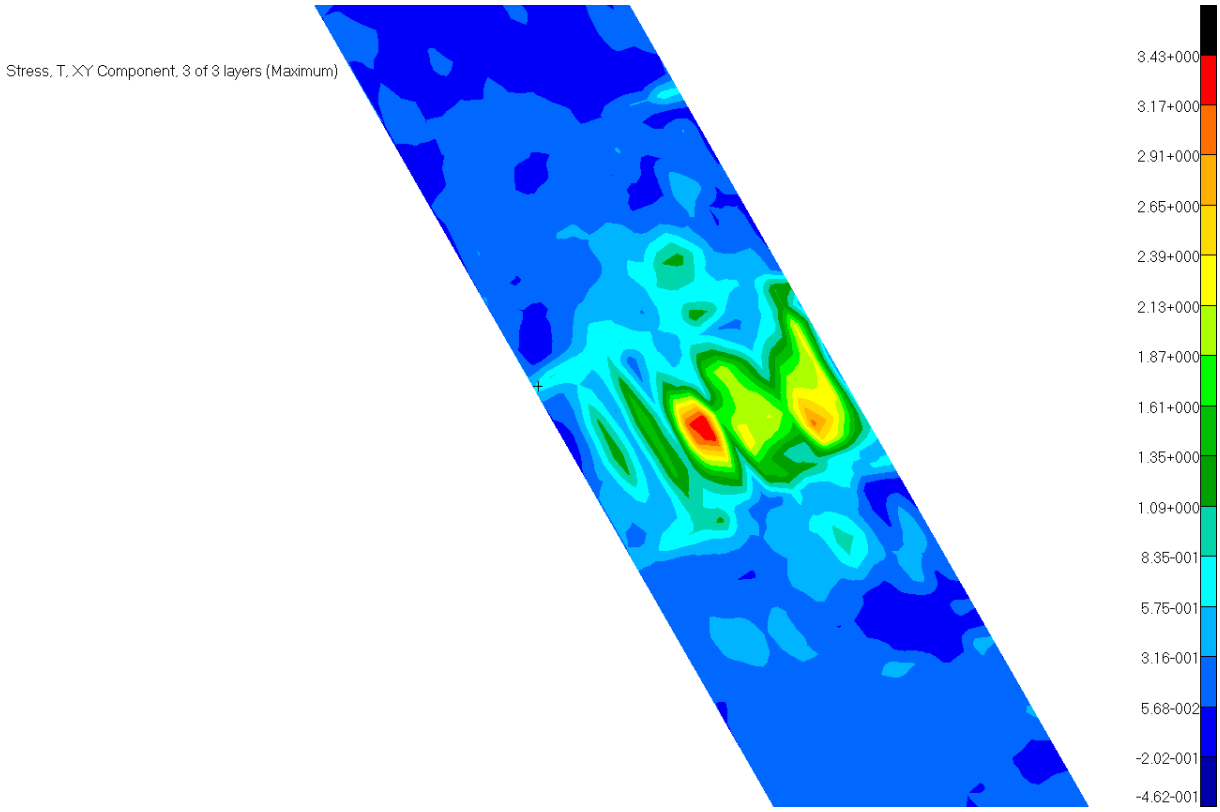

Figure 50 Slat stresses in shear

Slat displacements are shown below

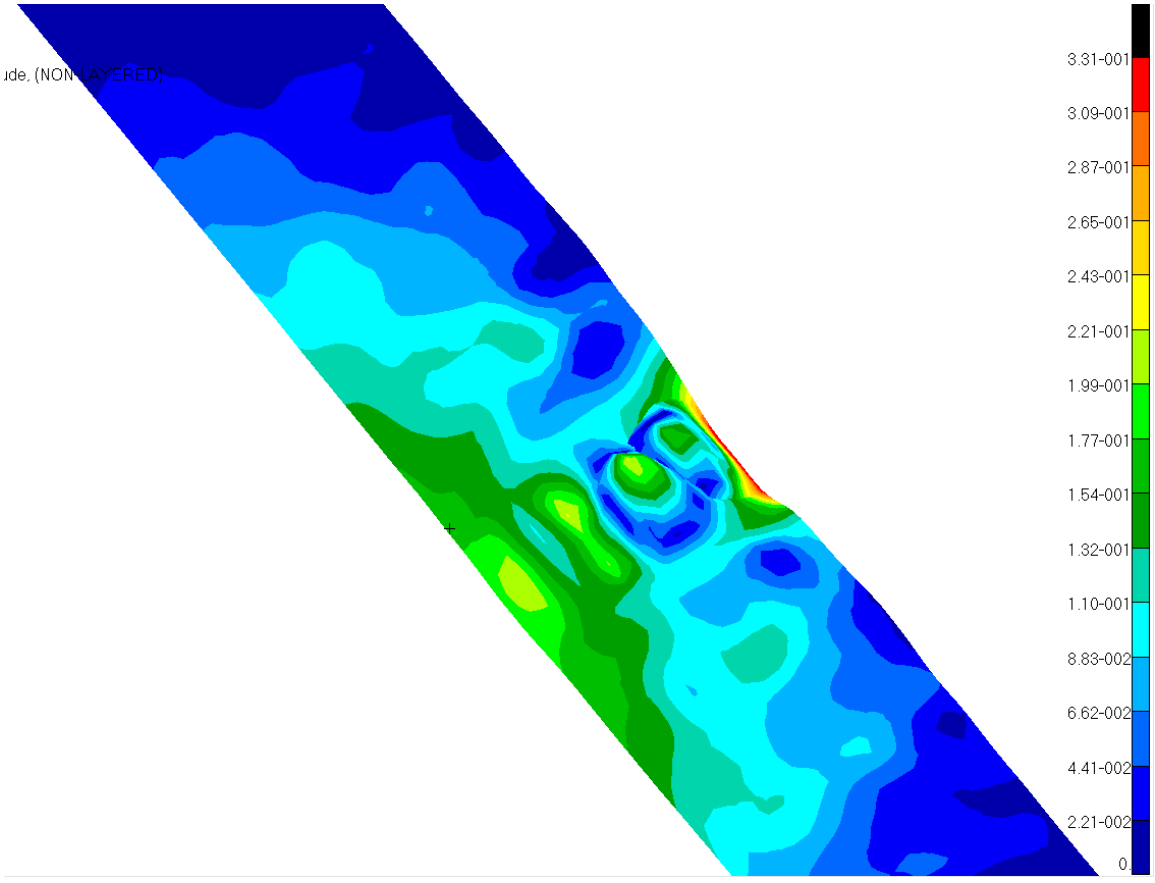

Figure 51 Slat displacements, view from the top

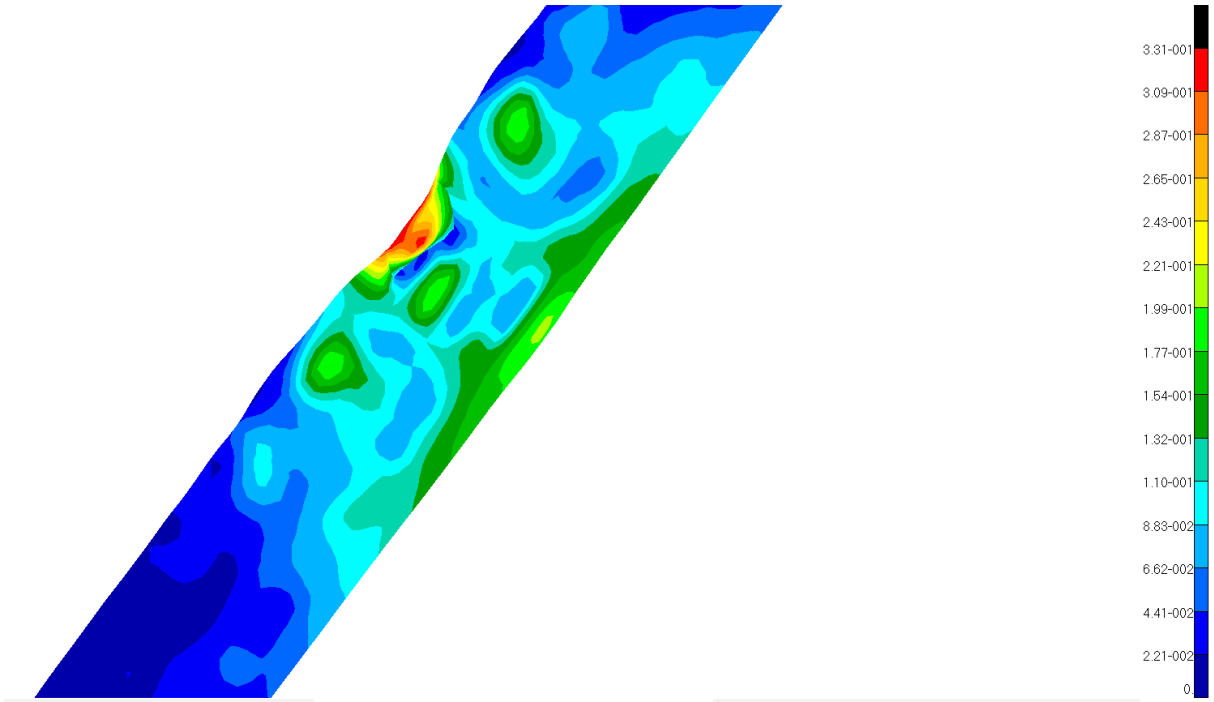

Figure 52 Slat displacements, view from the bottom

4.4 Simulation results assessment

Simulation showed that the bird strike cause relatively small stresses and displacements. Inasmuch the further slat structure modifications are not needed. The resulting slat stresses were calculated as a sum of static and "bird strike" stresses. Note, that the "bird strike" stresses were taken as maximum laminate stresses from inner, outer and middle plies of the skin thickness. This approach is conservative. According to this, the minimum reserve factor is 1.05 that corresponds to fiber compression failure mode. The minimum reserve factor allowed in this thesis is 1.10 but taking into account, that the factor 1.05 was obtained with conservative approach it is considered as allowable.

orientation	σ_t[MPa]	σ_c[MPa]	τ[MPa]
L	1215.3	1077.6	55.37
T	31.35	25.14	

Table 31 Ply 1 result stresses

orientation	RF_1	RF_2	RF_3
L	1.72	1.05	2.4
T	2.58	8.88	

Table 32 Ply 1 reserve factors

5 Conclusion

This thesis was focused on design and structural analysis of the composite wing leading edge slat of the Boeing 737-200 aircraft with respect to CS 25 requirements.

Bird strike simulation has shown that the bird strike causes relatively low stresses on the slat and it does not lead to failure of the structure. It is questionable because a real Wilbeck bird impact test made in [7] showed that the forward portion of the leading edge in the contact area was completely destroyed. However, the leading edge analyzed in [7] is rigidly fixed to the torsion box of the wing and cannot move. In turn, the slat designed in this paper is quite elastic and fixed only at five attachment points. Therefore, probably the current slat structure is able to damp the bird strike and not to fail. Animated result fringe proves that the slat structure is bouncing after a collision.

However, in order to make an overall conclusion it is needed to perform extensive amount of simulations, which is beyond the volume of the current work. Moreover, for the final assessment of the slat structure bird strike resistance it is necessary to perform series of full-size real tests. This is also beyond the scope of the current thesis.

6 Bibliography

[1] Georgiadis S, Gunnion AJ, Thomson RS, Cartwright BK, Bird-strike simulation for certification of the Boeing 787 composite moveable trailing edge, Victoria: Composite Structures, 2008.

[2] "EASA CM No.: EASA CM - S – 001 Issue: 01," European Aviation Safety Agency, Cologne, 2012.

[3] M. OSBORNE, "Single-Element Characterization of the LS-DYNA MAT54 Material Model," University of Washington, Washington, 2012.

[4] "MSC. NASTRAN Orthotropic Elastic (MAT8)," [Online]. Available: https://www.datapointlabs.com/TestPakDetails.asp?TestPakId=52. [Accessed 23 05 2015].

[5] SCHWEIZERHOF, K., K. WEIMAR a Th. ROTTNER, "Crashworthiness Analysis with Enhanced Composite Material Models in LS-DYNA - Merits and Limits," in *LS-DYNA World Conference*, Detroit, 1998.

[6] J. Cejpek, "Definition of Wing and Slat Loading," Institute of Aerospace Engineering, Faculty of Mechanical Engineering, Brno University of Technology, Brno, 2014.

[7] Rüdiger Keck, Wolfgang Machunze, Markus Kaden, "DESIGN, ANALYSIS AND MANUFACTURING OF A THERMOPLASTIC UD CF-PEEK SLAT," EADS Germany, Ottobrunn, 2012.

[8] B. Corp., "737-300 SYSTEM SCHEMATIC MANUAL: CHAPTER 27 FLIGHT CONTROLS," BOEING Corp., 2005.

[9] B. G. FALZON, "GARTEUR AG-28: IMPACT DAMAGE AND REPAIR OF COMPOSITE STRUCTURES," IMPERIAL COLLEGE LONDON, LONDON, 2006.

[10] В.В.Васильев, Механика конструкций из композиционных материалов, Москва: Машиностроение, 1988, pp. 130-144.

[11] Я.С.Карпов, Проектирование деталей и агрегатов из композитов, Харьков: ХАИ, 2010, pp. 64-67,101-103.

[12] R. Zubrytski, "Slat properties calculation," Brno, 2015.

[13] M. Guida, "Study, Design and Testing of Structural Configurations for the Bird-Strike Compliance of Aeronautical Components," University of Naples, Naples, 2008.

[14] M. V. Symonov, "Composite Wing Leading Edge Concept," Institute of Aerospace Engineering, Brno University of Technology, Brno, 2014.

[15] J. S.Wilbeck, "Impact Behaviour of Low Strength Projectiles," AIR FORCE MATERIALS LAB WRIGHT-PATTERSON AFB OH, 1978.

[16] S. Heimbs, "Computational methods for bird strike simulations: A review," Elsevier Ltd., Munich, 2011.

[17] MSC Software, Dytran 2013. User's Guide, 2014.

[18] Patran 2013. Interface To Dytran. Preference Guide, 2014.

7 List of figures

Figure 1 Single Element Mesh, Boundary Conditions, & Loading 12
Figure 2 Cross-Ply Simulations – Loading and Boundary Conditions 13
Figure 3 Stress vs. Strain – MAT58, longitudinal 13
Figure 4 Stress vs. Strain – MAT58, transversal 14
Figure 5 Stress vs. Strain – MAT58, cross-ply 14
Figure 6 Energy vs. Strain – MAT58, longitudinal 15
Figure 7 Energy vs. Strain – MAT58, transversal 15
Figure 8 Energy vs. Strain – MAT58, cross-ply 16
Figure 9 Stress vs. Strain – MAT8, longitudinal 18
Figure 10 Stress vs. Strain – MAT8, transversal 18
Figure 11 Stress vs. Strain – MAT8, cross-ply 19
Figure 12 Energy vs. Strain – MAT8, longitudinal 19
Figure 13 Energy vs. Strain – MAT8, transversal 20
Figure 14 Energy vs. Strain – MAT8, cross-ply 20
Figure 15 Final errors – comparison 23
Figure 16 Stress vs. Strain – MAT58, tensile test of a ±45° laminate 23
Figure 17 Stress vs. Strain – MAT8, tensile test of a ±45° laminate 24
Figure 18 Various concepts for composite slat design 25
Figure 19 Slat location 26
Figure 20 Slat CAD model 27
Figure 21 Attachment position in local CS 28
Figure 22 Take off configuration parameters 29
Figure 23 Wing continuous loading 30
Figure 24 Beam static analysis 30
Figure 25 Slat torsion moment 31
Figure 26 Composite rod geometrical parameters and loads 32
Figure 27 Shear stress flow 33
Figure 28 Composite rod geometrical parameters 34
Figure 29 Formulation of composite properties (according to [11]) 34
Figure 30 Ply 2 stresses, longitudinal 37
Figure 31 Ply 2 stresses, transversal 38
Figure 32 Ply 2 shear stresses 38
Figure 33 Slat X Membrane force, Eigenvalue λ = 1.201 39
Figure 34 Wing deflection, take-off load case 40
Figure 35 Slat deflections, take-off load case 40
Figure 38 The phases of bird influence (a) initial impact, (b) shock decay, (c) steady flow, and (d) pressure decay (according to [15]) 42
Figure 39 Lagrangian model: nodes are fixed to the material 43
Figure 40 Bird strike simulation on rigid plate with Lagrangian impactor model 43
Figure 41 Eulerian model: nodes stay fixed and material flows through the mesh 44
Figure 42 Bird strike simulation on rigid plate with Eulerian impactor model 44
Figure 43 ALE model: Eulerian mesh moves and deforms with material flowing inside 45
Figure 44 Bird strike simulation on rigid plate with ALE impactor model 45
Figure 45 SPH model: fluid is modelled by particles with free motion 46
Figure 46 SPH model 46

Figure 47 Bird strike simulation in Dytran....46
Figure 48 Slat stresses in tension, longitudinal 47
Figure 49 Slat stresses in compression, longitudinal....47
Figure 50 Slat stresses in tension, transversal 48
Figure 51 Slat stresses in compression, transversal....48
Figure 52 Slat stresses in shear....49
Figure 53 Slat displacements, view from the top 49
Figure 54 Slat displacements, view from the bottom 50

8 List of tables

Table 1 Toray T700GC-12K-31E/#2510 UD Tape Properties 12
Table 2 UD $[0]_{12}$ results - MAT58 16
Table 3 UD $[90]_{12}$ results - MAT58 17
Table 4 Cross-ply results - MAT58 17
Table 5 UD $[0]_{12}$ results - MAT8 21
Table 6 UD $[90]_{12}$ results - MAT8 21
Table 7 Cross-ply results - MAT58 21
Table 8 Summary of errors – longitudinal 22
Table 9 Summary of errors – transversal 22
Table 10 Summary of errors – cross ply 22
Table 11 Summary of errors – mean 22
Table 12 Summary of errors – final 22
Table 13 IM7/8552 material properties 28
Table 14 Beam continuous loading 29
Table 15 Beam loads 31
Table 16 Internal cross-sections l load factors 35
Table 17 Plies elastic constants, 45° plies 35
Table 18 Plies elastic constants, -45° plies 35
Table 19 Plies elastic constants, 0° plies 35
Table 20 Laminate properties 35
Table 21 Laminate stresses 36
Table 22 Ply stress in local CS 12, 45° plies 36
Table 23 -45° 36
Table 24 0° 36
Table 25 Ply reserve factors 36
Table 26 Ply 2 stresses 37
Table 27 Ply 2 reserve factors 37
Table 28 Attachments translations, take-off load case 39
Table 29Ply 1 stresses 41
Table 30Ply 1 reserve factors 41
Table 31 Ply 1 result stresses 50
Table 32 Ply 1 reserve factors 50

9 Appendix

Analyzed slat model properties

```
Material 1 - 2D ORTHOTROPIC Material
  Type 2D ORTHOTROPIC  Color 55    Layer 1           #Prop/Ply 24
          Density 1.45E-9        Damping 0.          Ref Temp 0.
          Tsai-Wu 0.
STIFFNESS      E1 158830.            G12 4800.            Nu12 0.36
               E2 9100.              G1z 4290.
                                     G2z 3190.
STRENGTH Tension1 2095.71      Compress1 1126.39         Shear 133.5
         Tension2 81.          Compress2 223.2
THERMAL   Alpha11 0.                 K11 0.               K12 0.
          Alpha22 0.                 K22 0.               K13 0.
                                     K33 0.               K23 0.
        Spec Heat 0.
OPTICAL   Front   Off           Reverse  Off

Property 1 - LAMINATE PLATE Property
  Type LAMINATE PLATE  Color 110   Layer 1        Material 0        #Elem 1361
  Laminate Option    As Specified
  Failure Theory  NONE     Bond Shear Allowable 0.
  Ref Temp    0.           Damping Coef 0.
  NS Mass/Area 0.           Bottom Surf ON 0.75
  Layup 1 -
    Ply  1  Material 1        Thickness 0.125              Angle 45.
    Ply  2  Material 1        Thickness 0.125              Angle 315.
    Ply  3  Material 1        Thickness 0.125              Angle 45.
    Ply  4  Material 1        Thickness 0.125              Angle 315.
    Ply  5  Material 1        Thickness 0.125              Angle 45.
    Ply  6  Material 1        Thickness 0.125              Angle 315.
    Ply  7  Material 1        Thickness 0.125              Angle 315.
    Ply  8  Material 1        Thickness 0.125              Angle 45.
    Ply  9  Material 1        Thickness 0.125              Angle 315.
    Ply 10  Material 1        Thickness 0.125              Angle 45.
    Ply 11  Material 1        Thickness 0.125              Angle 315.
    Ply 12  Material 1        Thickness 0.125              Angle 45.
Property 2 - LAMINATE PLATE Property
  Type LAMINATE PLATE  Color 110   Layer 1        Material 0        #Elem 11448
  Laminate Option    As Specified
  Failure Theory  NONE     Bond Shear Allowable 0.
  Ref Temp    0.           Damping Coef 0.
  NS Mass/Area 0.           Bottom Surf ON 0.75
  Layup 2 -
    Ply  1  Material 1        Thickness 0.125              Angle 45.
    Ply  2  Material 1        Thickness 0.125              Angle 315.
    Ply  3  Material 1        Thickness 0.125              Angle 0.
    Ply  4  Material 1        Thickness 0.125              Angle 45.
    Ply  5  Material 1        Thickness 0.125              Angle 315.
    Ply  6  Material 1        Thickness 0.125              Angle 0.
    Ply  7  Material 1        Thickness 0.125              Angle 0.
    Ply  8  Material 1        Thickness 0.125              Angle 315.
    Ply  9  Material 1        Thickness 0.125              Angle 45.
    Ply 10  Material 1        Thickness 0.125              Angle 0.
    Ply 11  Material 1        Thickness 0.125              Angle 315.
    Ply 12  Material 1        Thickness 0.125              Angle 45.

Load Set 1 - Combined Set
Referenced Sets
 Overall Scale   1.
 Set Scale       1.          10..NASTRAN 10
 Set Scale       1.          40..NASTRAN GRAV 40
Load Set 10 - NASTRAN 10
Load Set 10 - NASTRAN 10
Load Set 10 - NASTRAN 10
 Offset From Absolute Zero        0.
 Stefan-Boltzmann Constant        0.
 Alternate Form Free Convection   0
 Free Convection Exponent         0.
 Alternate Form Forced Convection 0
 Exclude Convective Energy Flow   0
 Fluid Conductivity               0.                  0 - None
 Fluid Specific Heat              0.                  0 - None
 Fluid Viscosity                  0.                  0 - None
 Fluid Density                    0.
```

```
 Constant Coefficient             0.
 Reynolds Number Exponent         0.
 Prandtl Exponent (into fluid)    0.
 Prandtl Exponent (out of fluid)  0.
Load Set 10 - NASTRAN 10
Nodal Forces (on Node)
      ID  Color    Layer   Def CS       X          Y          Z          Phase
      152    10        1        0         0.   1181.536         0.          0.
      164    10        1        0         0.   1313.192         0.          0.
      176    10        1        0         0.   1443.536         0.          0.
      188    10        1        0         0.   1572.566         0.          0.
      200    10        1        0         0.   1700.283         0.          0.
      212    10        1        0         0.   1826.688         0.          0.
      224    10        1        0         0.   1951.779         0.          0.
      236    10        1        0         0.   2075.557         0.          0.
      248    10        1        0         0.   2798.022         0.          0.
      260    10        1        0         0.   2319.174         0.          0.
      272    10        1        0         0.   2439.013         0.          0.
      284    10        1        0         0.   2557.539         0.          0.
      296    10        1        0         0.   2674.753         0.          0.
      308    10        1        0         0.   2790.653         0.          0.
      320    10        1        0         0.    2905.24         0.          0.
      332    10        1        0         0.   2752.459         0.          0.
Load Set 20 - NASTRAN 20
Load Set 20 - NASTRAN 20
Load Set 20 - NASTRAN 20
 Offset From Absolute Zero        0.
 Stefan-Boltzmann Constant        0.
 Alternate Form Free Convection   0
 Free Convection Exponent         0.
 Alternate Form Forced Convection 0
 Exclude Convective Energy Flow   0
 Fluid Conductivity               0.                  0 - None
 Fluid Specific Heat              0.                  0 - None
 Fluid Viscosity                  0.                  0 - None
 Fluid Density                    0.
 Constant Coefficient             0.
 Reynolds Number Exponent         0.
 Prandtl Exponent (into fluid)    0.
 Prandtl Exponent (out of fluid)  0.
Load Set 20 - NASTRAN 20
Nodal Forces (on Node)
      ID  Color    Layer   Def CS       X          Y          Z          Phase
     1764    10        1        0         0.       702.         0.          0.
     1781    10        1        0         0.       746.         0.          0.
     1798    10        1        0         0.       790.         0.          0.
     1836    10        1        0         0.       833.         0.          0.
     1853    10        1        0         0.       877.         0.          0.
     1870    10        1        0         0.       920.         0.          0.
     1925    10        1        0         0.       962.         0.          0.
     1989    10        1        0         0.      1004.         0.          0.
     2022    10        1        0         0.      1046.         0.          0.
     2069    10        1        0         0.      1088.         0.          0.
     2150    10        1        0         0.      1130.         0.          0.
     2223    10        1        0         0.      1171.         0.          0.
     2596    10        1        0         0.      1212.         0.          0.
     3062    10        1        0         0.      1252.         0.          0.
     3302    10        1        0         0.      1293.         0.          0.
     3472    10        1        0         0.      1216.         0.          0.
Load Set 30 - NASTRAN 30
Load Set 30 - NASTRAN 30
Load Set 30 - NASTRAN 30
 Offset From Absolute Zero        0.
 Stefan-Boltzmann Constant        0.
 Alternate Form Free Convection   0
 Free Convection Exponent         0.
 Alternate Form Forced Convection 0
 Exclude Convective Energy Flow   0
 Fluid Conductivity               0.                  0 - None
 Fluid Specific Heat              0.                  0 - None
 Fluid Viscosity                  0.                  0 - None
 Fluid Density                    0.
 Constant Coefficient             0.
 Reynolds Number Exponent         0.
 Prandtl Exponent (into fluid)    0.
 Prandtl Exponent (out of fluid)  0.
Load Set 30 - NASTRAN 30
Nodal Forces (on Node)
```

ID	Color	Layer	Def CS	X	Y	Z	Phase
1773	10	1	0	0.	966.	0.	0.
1790	10	1	0	0.	1092.	0.	0.
1806	10	1	0	0.	1214.	0.	0.
1845	10	1	0	0.	1333.	0.	0.
1862	10	1	0	0.	1448.	0.	0.
1878	10	1	0	0.	1560.	0.	0.
1980	10	1	0	0.	1669.	0.	0.
1997	10	1	0	0.	1774.	0.	0.
2052	10	1	0	0.	1875.	0.	0.
2086	10	1	0	0.	1973.	0.	0.
2158	10	1	0	0.	2067.	0.	0.
2584	10	1	0	0.	2158.	0.	0.
2954	10	1	0	0.	2246.	0.	0.
3182	10	1	0	0.	2330.	0.	0.
3422	10	1	0	0.	2410.	0.	0.
3542	10	1	0	0.	2269.	0.	0.

Load Set 40 - NASTRAN GRAV 40
Load Set 40 - NASTRAN GRAV 40
Body Loads
 Body Loads in Coordinate System 0
 Acceleration - Translational X 0. Y -9.80665 Z 0.

Constraint Set 1 - NASTRAN SPC 1
Constraints

Node ID 1	DOF 12---6	CSys 0	Color 120	Layer 1
Node ID 9	DOF 12---6	CSys 0	Color 120	Layer 1
Node ID 14	DOF 12---6	CSys 0	Color 120	Layer 1
Node ID 13063	DOF 123--6	CSys 0	Color 120	Layer 1
Node ID 13066	DOF 12---6	CSys 0	Color 120	Layer 1